

UNIVERSITY OF CALIFORNIA,  
IRVINE

Non-Aqueous Phase Drop Formation and Migration in a Uniform Water Saturated  
Fracture

THESIS

Submitted in partial satisfaction of the requirements for the degree of

MASTER OF SCIENCE

in Civil Engineering

Emphasis in Environmental Engineering

by

Kent Michael Pumphrey

Thesis Committee:  
Professor Constantinos Chrysikopoulos, Chair  
Professor Jan Scherfig  
Professor Brett Sanders

2002



The thesis of Kent Michael Pumphrey is approved:

---

---

---

Committee Chair

University of California, Irvine  
2002

# TABLE OF CONTENTS

	<i>Page</i>
LIST OF FIGURES	v
ACKNOWLEDGEMENTS	vi
ABSTRACT OF THE THESIS	vii
INTRODUCTION	1
CHAPTER 1: Drop formation in a fractured medium	6
CHAPTER 2: Definition of forces acting on a forming drop	8
2A: Buoyancy Force	9
2B: Momentum Flux Force	10
2C: Viscous Drag Force	11
2D: Surface Tension Force	13
2E: Induced Inertial Force	14
2F: Drop's Inertial Force	15
CHAPTER 3: Drop motion during formation stages	16
CHAPTER 4: Dimensionless variables	17
CHAPTER 5: Final drop size analysis	19
CHAPTER 6: Drop size results and discussion	21
CHAPTER 7: Drop motion within a fracture	27
CHAPTER 8: Advection dispersion equation for a migrating NAPL drop	30
CHAPTER 9: Solution of the advection dispersion equation for a moving drop	36
CHAPTER 10: Drop and contaminant plume motion results and discussions	40

## TABLE OF CONTENTS

	<i>Page</i>
SUMMARY AND CONCLUSIONS	47
NOTATIONS	50
REFERENCES	53

## LIST OF FIGURES

		<u>Page</u>
Figure 1	Schematic illustration of a NAPL drop forming within a uniform, water saturated fracture	7
Figure 2	Macroscopic forces acting on a NAPL drop	9
Figure 3	Schematic representation of the drop neck geometry at the neck/fracture wall interface	14
Figure 4	Schematic representation of a drop during the expansion stage	20
Figure 5	Comparison of model predictions and experimental data	23
Figure 6	Comparison of the drop ratio, $\bar{r}$ , with a changing aperture ratio, $\bar{d}$ , for TCE and DCM.	24
Figure 7	Comparison of $\bar{r}$ with a changing NAPL flow rate ratio, $\bar{Q}_d$ , for TCE and DCM.	26
Figure 8	Macroscopic forces acting on a drop moving within a fracture	28
Figure 9	Drop geometry used for modeling the NAPL source	33
Figure 10	Coordinate system centered and moving with the drop	35
Figure 11	TCE plumes generated from a single drop within a horizontal fracture at four specific times	44
Figure 12	TCE plumes generated from a single drop within a fracture at four specific longitudinal velocities	46

## **ACKNOWLEDGMENTS**

I would like express my thanks to my committee chair, Professor Constantinos Chrysikopoulos, whose patients and guidance allowed me complete this work to the best of my abilities. I also would like to thank my committee member, Professor Brett Sanders for his thorough review of my work and his insightful comments help strengthen this work.

## **ABSTRACT OF THE THESIS**

Non-Aqueous Phase Drop Formation and Migration in a Uniform Water Saturated

Fracture

By

Kent Michael Pumphrey

Master of Science in Civil Engineering

University of California, Irvine, 2002

Professor Constantinos Chrysikopoulos, Chair

A theoretical model was developed for determining the size of a non aqueous phase liquid drop (NAPL) forming within a parallel wall fracture. The drop's final size is dependent on the drop's motion during its formation. The model was developed by first defining the macroscopic forces acting on the drop during its formation within the fracture and then applying Newton's 2<sup>nd</sup> Law to determine its motion. The final drop size was determined by calculating the moment the drop moves far enough to separate from its NAPL source. This calculation was done using a 4<sup>th</sup> order Runge-Kutta numerical method on the drop's equations of motion. The drop diameters calculated were on the order of 1.5 times the NAPL entrance aperture dimension. The model was also compared to available experimental results and showed satisfactory agreement.

A theoretical two dimensional model was also developed for the motion of the drop and the transient contaminant plume resulting from the dissolution of a single

component NAPL drop moving within a water saturated fracture with an aperture much larger than the diameter of the drop. A solution was derived for the longitudinal and normal terminal velocities of a single drop moving within a fracture and was calculated by equating the drop's buoyancy force to the drag force acting on the drop. A time and space dependant solution for the two-dimensional advection dispersion equation was obtained by assuming the drop, and the contaminant plume generated by the drop, are significantly smaller than the fracture's aperture and therefore do not interact with the fracture walls. An analytical solution was obtained by performing two separate Fourier transform, one with respect to the fracture's longitudinal axis and the other with respect to the axis normal to the fracture's walls. A TCE drop of 1  $\mu\text{m}$  radius generated stable contaminant plumes dimensions, at solute concentrations of 5ppm, which were on the order of 600 mm. These plumes are significantly larger than the drop and aperture of the fracture, therefore the assumption that the drop's contaminant plume will not interact with the fracture walls is false and that the fracture walls must be taken into account when analyzing this system.

## INTRODUCTION

Non-aqueous phase liquids (NAPLs) have played a large role in contaminating aquifers through out much of the industrial world [*Bellma and Kueper, 1999*]. These contaminants typically consist of immiscible organic liquids, such as trichloroethylene (TCE), tetrachloroethylene (PCE), and have been in use since the 1940's in industries such as dry cleaning, metal degreasing, printing and photographic operations [*Bellma and Kueper, 1999*]. Past releases of NAPLs into the sub-surface have contaminated thousands of sites through out the industrialized world and have created quite a concern among communities due to the health risks generated by contaminated public drinking water. NAPLs typically have a low water solubility (PCE, for example, has a water solubility of 150mg/L at 25° C) and concentrations of PCE as low as 5 ppm can create a health hazard when contained in drinking water [*Fetter, 1993*]. Subsurface contamination coupled with the difficulties associated with removing NAPLs from any contaminated aquifer make it imperative that research continues in order to understand fully on how NAPLs interact within the subsurface so that appropriate remediation solutions maybe obtained.

The movement of NAPL contaminants within a water saturated fractured media has become a topic of significant research in recent years. Large portions of the industrialized areas of North America and Europe are located in geologic areas where the underlying strata is made-up of large arrays of surface or near surface fractured bedrock, such as sandstone or igneous rock [*Parker et al., 1994*]. Because of the industrial activities in these areas there is an increased risk of subsurface contamination due to accidental spills or intentional deposits of contaminants into the surrounding environment. When a NAPL enters into the subsurface, it migrates as a separate phase

downward through the unsaturated zone and into the saturated zone. If the subsurface contains an array of fractures, the contaminant will prefer to migrate into these fractures and use these as a means for movement within the subsurface medium. This preference greatly enhances the motion of the contaminant helping the NAPL to move quicker and deeper into the subsurface and thus contaminating larger portions of bedrock. Any increase in the NAPL spreading will make it much more difficult to remove it from the subsurface and will create a persistent and continuous source of aqueous phase contamination for a long period of time [VanderKwaak and Sudicky, 1996]. Therefore, a more thorough understanding of the mechanisms involved in NAPL migration within a fractured geologic medium is essential in determining the best means for dealing with the remediation of a contaminated fractured formation.

Ground water movement and contaminant transport is different within a fractured geologic material when compared to a porous medium. In a fractured medium, the ground water, and any immiscible liquids contained within, tend to move only within the fractures themselves and migrate throughout the fracture array. A NAPL is less likely to disperse out of the fracture and into the surrounding bedrock due to a saturated hydraulic conductivity value that is several orders of magnitude larger than the saturated hydraulic conductivity value of any rock matrix [Abdel-Salam and Chrysikopoulos, 1996]. The fracture's larger relative hydraulic conductivity provides an easier flow path for the water, plus its entrained contaminants, to move through. This creates a situation where the ground water and entrained NAPL will prefer to stay within the fractures and not migrate into the bedrock. Also the groundwater flow rates are typically higher within fractures when compared to groundwater flow rates within aquifers. This allows the contaminants to migrate at higher velocities when traveling in

a fracture array and to spread faster and consequently to migrate longer distances.

Ground water and the entrained contaminants also have the potential of infiltrating a much larger bulk volume of fractured geological formation, when compared to a non-fractured porous medium. A typical fractured geological medium contains a volume of void space that can range from 1% to .001% of the total bulk volume. This value is considerable less than a typical rock matrix porosity, which can range anywhere from 34% to 60% for clays or 5% to 30% for sandstone rocks [*Domenico and Schwartz, 1990*]. Therefore, a much larger volume of fractured medium, as compared to a non-fractured porous medium, is required in order to create an equivalent amount of void volume [*Feenstra and Cherry, 1988*]. Because groundwater and contaminants can only move within these void spaces, a given volume of contaminant released into a fractured medium will penetrate deeper and spread farther than a comparable release into a porous medium.

There have been several recent papers on contaminant transport in fractured rock with the majority focusing on the migration of contaminant plumes by means of ground water movement within a fracture network. Publications by VanderKwaak and Sudicky [*1996*], Parker et al. [*1994*] and Rubin et al. [*1997*] analyze the rates of NAPL dissolution into the aqueous phase and subsequent contaminant movement within the rock fractures by means of a fracture network. These works begin with the assumption that a NAPL either exists in a state of residual saturation along the fracture walls or that they pool at higher than residual saturation in areas which are connected to these fractures. Either way, the NAPL's only means of migration is to slowly dissolve into the ground water and to spread within the fractured rock by way of a contaminant plume which exists at either the NAPL's aqueous saturation concentration or lower.

The possibility of a NAPL migrating within a fracture network as a separate phase, as in the form of drops, is not considered in their analysis.

Recent research has also been conducted on the effects of colloid suspensions in aiding the movement of NAPL solutes within a fractured medium. In a water saturated fracture, dissolved NAPL may sorb onto any solid surface, such as the solid particles which may be entrained within the water flowing through the fracture. The work by James and Chrysikopoulos [1999, 2000], Abdel-Salam and Chrysikopoulos [1994] and Chrysikopoulos and Abdel-Salam [1997] examine the effects of the various colloid interactions within a fractured medium and how these interactions change the rate of solute migration. Solute migration can be either enhanced by the action of the solute sorbing onto a moving particle or retarded if the colloids collect large quantities of solute and either are sorbed onto the fracture walls or diffuse into the solid matrix at a high rate. All of these mentioned works examine the motion of a solute after the NAPL source has dissolved into the groundwater, creating a migrating plume whose existence is measured by the water's solute concentration. These works neglect the possibility that the NAPL itself, by forming drops, can migrate as a separate phase within the confines of a fracture and contribute to significant contamination deep within the rock matrix.

One additional means of contaminant migration within a fractured medium is by the migration of NAPL drops contained within the moving groundwater. A NAPL source can enter into a fracture either from pore channels or other smaller fractures that are connected to the main fracture. The contaminant may enter into a fracture as long as the net macroscopic force acting on the NAPL is directing it into the fracture. Once the NAPL enters the fracture it can do one of two things: form a thin layer which spreads

along the wall of the fracture or form a drop which detaches from the fracture's wall and enters into the fracture's interstitial flow field. The final form that the NAPL eventually takes is dependent on both the magnitude and direction of the various forces acting on the NAPL as it enters into the fracture. The more these forces direct the NAPL away from the fracture wall the more likely a drop will be created.

If a drop does form it will continue to grow in size so long as it stays connected to its NAPL source, and will reach its final size when it finally detaches from this source. The longer the drop is attached to its source location the larger the drop becomes. How long a drop stays attached to its source depends on several physical properties including the fracture's interstitial flow rate, NAPL density, NAPL inflow rate and surface tension. Small drops, once they become detached, will begin to migrate within the fracture driven by the buoyancy of the drop and the interstitial fluid flow moving within the fracture and eventually landing somewhere deep within the fractured bedrock. Drops, which are as large as the fracture's aperture or larger, will move differently than the smaller drops because the larger drops cannot completely separate themselves from the fracture walls and will all but block the interstitial fluid moving within the fracture. Drops of this size will travel as a slug flow and can be examined as such. Regardless of the drop's final size, the formation and detachment of drops within fractures can provide an additional means of transporting a significant amount of NAPL as a separate phase within a geologic formation and greatly add to the contamination of the medium. Not only is the NAPL migrating within the fracture as a separate phase it is also increasing the amount of contamination by dissolving into the moving interstitial fluid and creating a contaminant plume. NAPL drop formation, motion and the contaminant plume these drops generate within the domain of a fracture medium has

not been analyzed in the literature, therefore it is the intent of this work to explore this combined physical problem.

## **1. Drop formation in a fractured medium**

The formation of a liquid drop contained within a moving fluid is a complicated, three-dimensional process involving moving and evolving two-phase fluid interfaces [Kim *et al.*, 1994]. Typically a problem such as this is usually examined from a microscopic viewpoint using Navier-Stokes equation so that all effects created by any small fluctuations at the drop's interface are captured. However, if both fluids are at Reynolds numbers of approximately one or less the analysis of this process can be simplified greatly. The reason for the simplification is that at these flow conditions a drop's surface will not distort, and the drop will act as if it were a solid sphere with no detectable deformation of its shape [White, 1991]. This allows the drop formation process to be modeled within a macroscopic reference frame by using Newton's 2<sup>nd</sup> Law of Motion as the drop's final size is fully dependent on the drop's motion during the formation stages. By assuming the drop's shape remains spherical throughout the life of the drop, all of the forces acting on the forming drop can be defined and the drop's motion can be determined from Newton's 2<sup>nd</sup> Law.

NAPL drop formation occurs in two distinct phases beginning with the expansion stage and ending with the detachment phase [Kuloor and Kumar, 1990]. The expansion stage of drop development begins when the NAPL initially enters the fracture and starts to form a drop. The growing drop will form a neck connecting the body of the drop to the NAPL entrance point as shown in Figure 1. This enables the NAPL to continuously feed into the drop allowing the drop to grow. If there is any moving water inside the fracture, the drop will migrate along the fracture wall driven

by the flowing water. The expansion stage continues as long as the drop's neck remains intact with its NAPL source and the drop's base remains in constant contact with the fracture wall as the drop moves along it. This stage ends when either the drop severs its neck or, with the neck still intact, the drop's base begins to lift from the fracture wall.

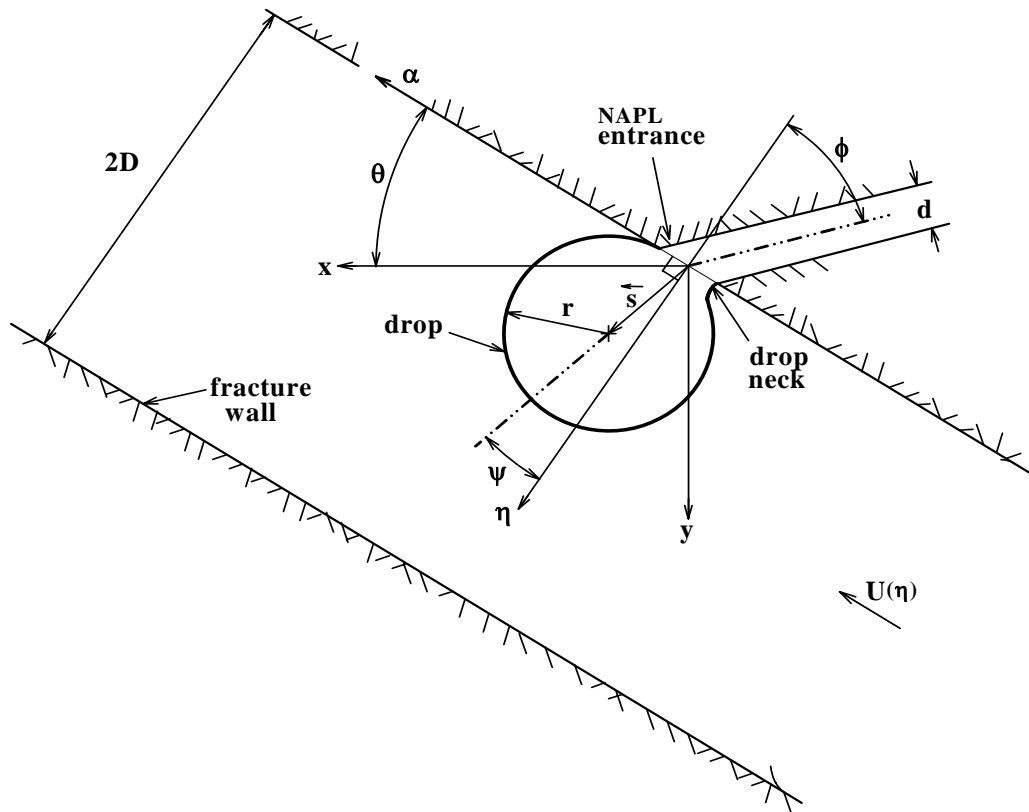


**Figure 1. Schematic illustration of a NAPL drop forming within a uniform, water saturated fracture.**

The detachment stage begins when a drop either severs its neck or when the drop, which is still connected to its material source, begins to lift from the fracture wall. The lifting of the drop away from the fracture wall occurs when the normal component of the net macroscopic forces acting on the drop is directed into the fracture and away from the fracture wall. During this stage the drop begins to move away from its source

and continues to grow because it is still connected to the NAPL source point by its thinning neck. Drop formation and the detachment stage are complete when the drop severs its connecting neck and enters into the main fracture's flow regime.

## 2. Definition of forces acting on a forming drop

The final size of a forming NAPL drop is dependent the macroscopic forces acting on the drop, therefore these forces need to be defined. The definition of these forces are as follows (see Figure 2)

$\vec{F}_B \equiv$  Buoyancy Force due to the differences in fluid densities,

$\vec{F}_D \equiv$  Viscous Drag Force acting on the drop generated by the shearing interactions occurring at the drop/water interface,

$\vec{F}_I \equiv$  Induced Inertial Force generated by the encroaching drop into the water phase,

$\vec{F}_M \equiv$  Added Momentum due to the NAPL influx,

$\vec{F}_S \equiv$  Surface Tension Force acting at the drop/fracture wall interface.

Newton's 2<sup>nd</sup> Law will be used in determining the motion of the drop during both the expansion stage and the detachment stages. Newton's 2<sup>nd</sup> Law is defined as

$$\vec{F} = \vec{F}_B + \vec{F}_D + \vec{F}_I + \vec{F}_M + \vec{F}_S, \quad (1)$$

where  $\vec{F}$  represents the drop's inertial force. In order to use Newton's 2<sup>nd</sup> Law each individual force shall be defined in detail.

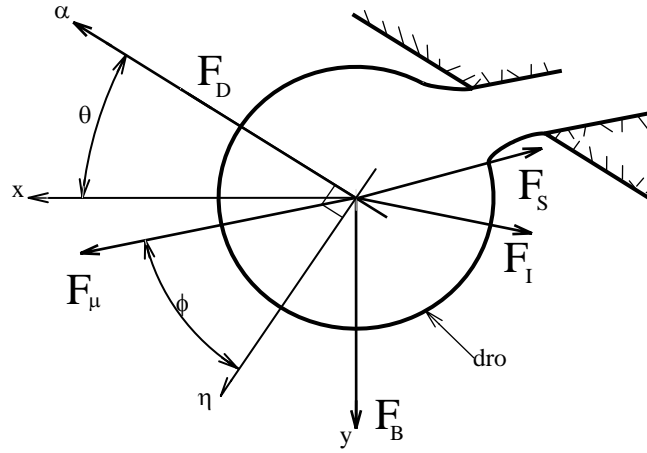


**Figure 2. Macroscopic forces acting on a NAPL drop**

**2A. Buoyancy Force,  $\vec{F}_B$**

A buoyancy force is created when the NAPL density differs from the density of the interstitial fluid. This force is defined as

$$\vec{F}_B = \nabla_d g(\rho_d - \rho_w)\hat{y}, \quad (2)$$

where  $\nabla_d$  is the drop volume,  $\rho_d$  is the NAPL drop density,  $\rho_w$  is the water density,  $g$  is the gravitational acceleration constant and  $\hat{y}$  is the unit vector in the y direction. At low Reynolds numbers, a NAPL drop will assume a spherical shape and remains so through out both the expansion and detachment phase of the growth process. Experiments have shown that a NAPL drop maintains a spherical shape for drop-to-containment ratios as large as 0.60 [Borhan and Pallinti, 1998]. Therefore, the radius of a drop can be calculated, once the volume is known, by using the equation of a sphere's volume. Determining the drop's volume at any time during the drop's formation process can be calculated from the following equation

$$\nabla_d = Q_d t, \quad (3)$$

where  $Q_d$  is the constant NAPL volumetric flow rate and  $t$  is time. This model's coordinate system will be aligned with the main fracture therefore the buoyancy force must be transformed to this system. The following equation performs this transformation

$$\hat{y} = \hat{\eta} \cos \theta - \hat{\alpha} \sin \theta, \quad (4)$$

where  $\hat{\eta}$  is the unit vector in the  $\eta$  direction,  $\hat{\alpha}$  is the unit vector in the  $\alpha$  direction and  $\theta$  is the fracture's angular offset. The coordinate  $\eta$  is the spatial coordinate normal to the fracture wall and  $\alpha$  is the spatial coordinate in the longitudinal direction. Substitution of the time relationship for the drop volume and transforming the buoyancy force equation to the desired coordinate system gives

$$\vec{F}_B = Q_d t g (\rho_d - \rho_w) (\hat{\eta} \cos \theta - \hat{\alpha} \sin \theta). \quad (5)$$

## 2B. Momentum Flux Force, $\vec{F}_m$

During the drop's formation period, momentum is constantly added to the drop by virtue of the steady influx of the NAPL. This momentum flux acts on the drop in the direction of influx and is assumed constant because the volumetric flow rate of the NAPL is assumed constant. The equation for the momentum flux force can be written as [Kim et al., 1994]

$$\vec{F}_m = Q_d^2 \frac{\rho_d}{A_f} (\hat{\eta} \cos \phi + \hat{\alpha} \sin \phi), \quad (6)$$

where  $A_f$  is the area of NAPL entrance point and  $\phi$  is the NAPL entrance angle. If the NAPL's entrance into the fracture is approximately circular, this area becomes

$$A_f = \frac{\pi}{4} d^2, \quad (7)$$

where  $d$  is the diameter of the NAPL entrance point. Substituting equation (7) into (6) gives

$$\vec{F}_m = \frac{4Q_d^2 \rho_d}{\pi d^2} (\hat{\eta} \cos \phi + \hat{\alpha} \sin \phi). \quad (8)$$

### 2C. Viscous Drag Force, $\vec{F}_D$

The viscous drag force acting on the drop is generated by the difference in velocities between the flowing water inside the fracture and the nearly stationary drop attached to the fracture wall. The generated velocity gradient, coupled with the fluid's viscosity, provide the necessary elements needed to generate the drag force. This force acts along the water/drop interface and in the direction of relative fluid motion. The expression for this force is [Kim *et al.*, 1994]

$$\vec{F}_D = \frac{1}{2} C_{dw} \rho_w \vec{U}_{eff} |U_{eff}| A_{eff}, \quad (9)$$

where  $C_{dw}$  is the drag coefficient for a bounded flow,  $\vec{U}_{eff}$  is the effective velocity vector,  $U_{eff}$  is the magnitude of the effective velocity between the water and the drop and  $A_{eff}$  is the effective area of the drop. The effective velocity can be stated as

$$\vec{U}_{eff} = \left( U_w - \frac{d\alpha_D}{dt} \right) \hat{\alpha}, \quad (10)$$

where  $\frac{d\alpha_D}{dt}$  is the drop's center velocity in the  $\alpha$  direction and  $U_w$  is the average water velocity in the fracture. The effective velocity does not have a component in the  $\eta$  direction because the water velocity is assumed to have only a longitudinal component and the drop does not have a vertical velocity component since it is attached to the fracture wall during its formation. The effective area of the drop is defined as

$$A_{eff} = \pi r^2, \quad (11)$$

where  $r$  is the drop's radius. The drag coefficient used by this model is a curve fitted value determined for an unbounded flow regime around a solid sphere and adjusted for use in a bounded flow problem. This adjustment is necessary since the confining walls of a fracture have an effect on total drag force exerted on an object. The value for the curve fitted drag coefficient for an unbounded flow about a sphere is [White, 1991]

$$C_D = \frac{24}{Re} + \frac{6}{1 + \sqrt{Re}} + 0.4 \quad 0 \leq Re \leq 10^5, \quad (12)$$

where  $Re$  is the Reynolds number for the interstitial fluid flowing within the fracture. This Reynolds number is defined as

$$Re = \frac{\rho_w U_{eff} 2r}{\mu_w}, \quad (13)$$

where  $\mu_w$  is the absolute viscosity of water. The drag coefficient for a bounded flow is defined by [Kim, 1992]

$$C_{dw} = \frac{C_D}{(1 - \bar{r}^2)^3}, \quad (14)$$

where  $\bar{r} = \frac{r}{D}$  and  $D$  is one half the fracture aperture. Substituting the values for  $A_{eff}$

(11) and  $U_{eff}$  (10) into (9) gives the desired expression for the viscous drag force

$$\vec{F}_D = \frac{\pi}{2} C_{dw} \rho_w r^2 \left( U_w - \frac{d\alpha_D}{dt} \right) \bigg| U_w - \frac{d\alpha_D}{dt} \bigg| \hat{\alpha}. \quad (15)$$

## 2D. Surface Tension Force, $\vec{F}_S$

The surface tension force acts on the drop at the drop/fracture wall connection point and tries to keep the drop attached to the fracture wall. This force is directed from the

center of the drop towards the drop/fracture connection point. Assuming that the drop's connection to the fracture wall is circular, the expression for this force is

$$\vec{F}_s = -\mu \vec{f}[\Psi], \quad (16)$$

where  $\mu$  is the surface tension coefficient and  $\vec{f}[\Psi]$  is a vector function which takes into account the angle of inclination between the drop's neck,  $\Psi$ , and the  $\eta$  axis which is normal fracture wall (see Figure 3). The function  $\vec{f}[\Psi]$  can be expressed as follows [Kim et al., 1994]

$$\vec{f}[\Psi] = \pi d \cos \Psi \frac{4\Psi}{\pi^2 - 4\Psi^2} \hat{\alpha} + \pi d \frac{\sin \Psi}{\Psi} \hat{\eta}, \quad (17)$$

where  $\alpha_D$  and  $\eta_D$  are the coordinates of the drop's center and

$$\cos \Psi = \frac{\eta_D^2}{\sqrt{\alpha_D^2 + \eta_D^2}}, \quad (18)$$

$$\sin \Psi = \frac{\alpha_D^2}{\sqrt{\alpha_D^2 + \eta_D^2}}. \quad (19)$$

Substituting equation (17) into (16) yields the final equation for the surface tension force

$$\vec{F}_s = -\mu \pi d \frac{\sin \Psi}{\Psi} \hat{\eta} - \mu \pi d \frac{4\Psi}{\pi^2 - 4\Psi^2} \cos \Psi \hat{\alpha}. \quad (20)$$

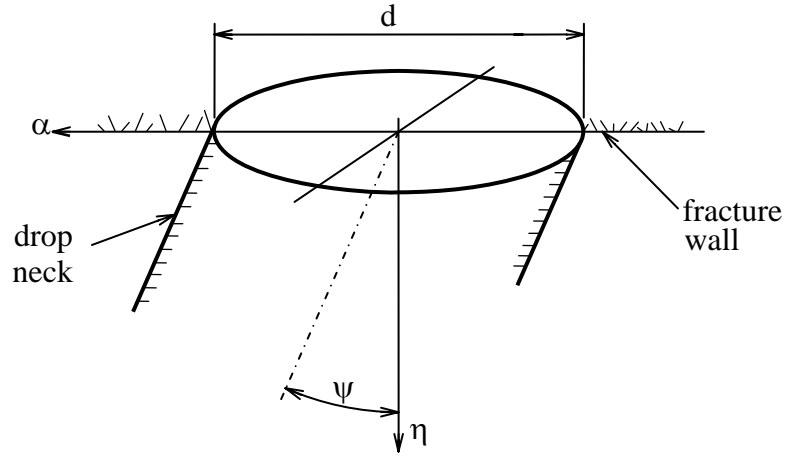


**Figure 3. Schematic representation of the drop neck geometry at the neck/fracture wall interface.**

**2E. Induced Inertial Force,  $\vec{F}_I$**

As the drop expands into the fracture, it displaces water by accelerating the nearby water away from the drop. This acceleration imposes a reaction force onto the drop acting in a direction opposite to the drop's motion. This force can be generated from Newton's 2<sup>nd</sup> Law

$$\vec{F}_I = -\frac{d}{dt} \left( M_r \frac{d\vec{s}}{dt} \right). \quad (21)$$

The reduced mass constant,  $M_r$ , quantifies the amount of water mass that is accelerated by the moving drop and is proportional to the mass of water displaced by the drop. This constant is defined by

$$M_r = C_m \rho_w Q_d t. \quad (22)$$

The reduced mass coefficient,  $C_m$ , is derived from analyzing the kinetic energy added to a fluid when a body passes through it [Kim, 1992]. The value of  $C_m$  used for a drop

expanding from a plate orifice is generally taken as  $\frac{11}{16}$  [Kim et al., 1994]. The drop's center position vector,  $\vec{s}$ , is defined as

$$\vec{s} = \eta_D \hat{\eta} + \alpha_D \hat{\alpha}. \quad (23)$$

Taking the time derivative of equation (23) and substituting the resulting expression into equation (21) yields

$$\vec{F}_I = -\frac{d}{dt} \left( M_r \left( \frac{d\eta_D}{dt} \hat{\eta} + \frac{d\alpha_D}{dt} \hat{\alpha} \right) \right). \quad (24)$$

Inputting equation (22) into (24) gives

$$\vec{F}_I = -C_m \rho_w Q_d \frac{d}{dt} \left( t \left( \frac{d\eta_D}{dt} \hat{\eta} + \frac{d\alpha_D}{dt} \hat{\alpha} \right) \right). \quad (25)$$

Taking the time derivative in equation (25) gives the final expression for the induced inertial force

$$\vec{F}_I = -C_m \rho_w Q_d \left( \frac{d\eta_D}{dt} + t \frac{d^2\eta_D}{dt^2} \right) \hat{\eta} - C_m \rho_w Q_d \left( \frac{d\alpha_D}{dt} + t \frac{d^2\alpha_D}{dt^2} \right) \hat{\alpha}. \quad (26)$$

## 2F. Drop's Inertial Force, $\vec{F}$

Following the same derivation method outlined in section 3E and using

$$M = \rho_d Q_d t \quad (27)$$

to represent the drop's mass yields the following expression for the drop's inertial force

$$\vec{F} = \rho_d Q_d \left( \frac{d\eta_D}{dt} + t \frac{d^2\eta_D}{dt^2} \right) \hat{\eta} + \rho_d Q_d \left( \frac{d\alpha_D}{dt} + t \frac{d^2\alpha_D}{dt^2} \right) \hat{\alpha}. \quad (28)$$

## 3. Drop motion during formation stages

The final drop size depends on the motion of the drop while its neck is still attached

to the NAPL source. The growth cycle of a drop begins when the NAPL enters the fracture and ends when the drop's neck severs the tie between NAPL source and the drop. The drop's final size can be determined if one knows the length of this growth cycle and the NAPL flow rate entering into drop. The moment at which the drop severs its connection to the NAPL source depends on both the size of the drop and how far the drop has moved away from its source point. Regardless of which formation stage the drop is in, when the distance from the center of the drop is great enough for separation to occur the formation process ends and the drop has reached its final size.

At low flow rates in a fracture a drop will sever its neck when the neck length becomes greater than or equal to the diameter of the NAPL entrance [Kuloor and Kumar, 1970]. This relationship is given as follows

$$\sqrt{\eta_D^2 + \alpha_D^2} - r \geq d. \quad (29)$$

In order to determine when a drop will separate from its source, the drop's displacement during formation must be calculated. The motion of the drop can be determined by solving equation (1) in both the  $\alpha$  and the  $\eta$  directions. Inserting equations (5), (8), (15), (20), (26) and (28) into (1) and simplifying gives

$\alpha$  - direction:

$$\begin{aligned} (\rho_d + C_m \rho_w) \left( \frac{d\alpha_D}{dt} + t \frac{d^2\alpha_D}{dt^2} \right) &= \frac{4\rho_d Q_d}{\pi d^2} \sin \phi - (\rho_d - \rho_w) g t \sin \theta - \\ &- \mu \pi d \frac{4\Psi \cos \Psi}{Q_d [\pi^2 - 4\Psi^2]} + \frac{\pi C_{dw}}{2Q_d} \rho_w r^2 \left( U_w - \frac{d\alpha_D}{dt} \right) \left| U_w - \frac{d\alpha_D}{dt} \right|, \end{aligned} \quad (30)$$

$\eta$  - direction:

$$\begin{aligned}
& (\rho_d + C_m \rho_w) \left( \frac{d\eta_D}{dt} + t \frac{d^2\eta_D}{dt^2} \right) = \\
& - \mu \pi d \frac{\sin \Psi}{Q_d \Psi} + \frac{4\rho_d Q_d}{\pi d^2} \cos \phi + (\rho_d - \rho_w) g t \cos \theta .
\end{aligned} \tag{31}$$

Equations (30) and (3) describe the motion of the drop's center as it exists in its developmental stages and are used together in order to calculate the center's coordinates. These coordinates are then used to check the validity of equation (29). The instant equation (29) becomes valid the drop has severed its neck and has reached its final size for the model parameters. The final drop size is calculated from

$$r_f = \sqrt[3]{\frac{3Q_d}{4\pi} t_f}, \tag{32}$$

where  $r_f$  is the final drop radius and  $t_f$  is the time when drop severs its neck.

#### 4. Dimensionless variables

Generally, it is more convenient to work in dimensionless variables. In the present work the following definitions will be employed

$$A_D = \frac{\alpha_D}{2D}, \tag{33}$$

$$H_D = \frac{\eta_D}{2D}, \tag{34}$$

$$T = \frac{tU_w}{2D}, \tag{35}$$

$$\bar{r} = \frac{r}{D}, \tag{36}$$

$$\bar{d} = \frac{d}{2D}, \tag{37}$$

$$\bar{\rho} = \frac{\rho_d}{\rho_w}, \quad (38)$$

$$\bar{Q}_d = \frac{Q_d}{\pi D^2 U_w} \quad (39)$$

$$\bar{\Psi} = \tan^{-1} \frac{A_D}{H_D}, \quad (40)$$

$$\cos \bar{\Psi} = \frac{H_D}{\sqrt{A_D^2 + H_D^2}}, \quad (41)$$

$$\sin \bar{\Psi} = \frac{A_D}{\sqrt{A_D^2 + H_D^2}}, \quad (42)$$

$$F_r = \frac{\rho_w U_w^2}{2D(\rho_w - \rho_d)g} \text{ Froude number,} \quad (43)$$

$$W_e = \frac{\rho_w U_w^2 2D}{\mu} \text{ Weber number.} \quad (44)$$

The model equations (29) - (32) become

$$\sqrt{H_D^2 + A_D^2} - \frac{1}{2} \bar{r} \geq \bar{d}, \quad (45)$$

$$\begin{aligned} (\bar{\rho} + C_m) \left( \frac{dA_D}{dT} + T \frac{d^2 A_D}{dT^2} \right) &= \frac{\bar{C}_{dw} \bar{r}^2}{2\bar{Q}_d} \left( 1 - \frac{dA_D}{dT} \right) \left| 1 - \frac{dA_D}{dT} \right| - \\ &- 16 \frac{\bar{d}}{W_e \bar{Q}_d} \frac{\bar{\Psi} \cos \bar{\Psi}}{[\pi^2 - 4\bar{\Psi}^2]} + \frac{\bar{\rho} \bar{Q}_d}{\bar{d}^2} \sin \phi + \frac{T}{F_r} \sin \theta, \end{aligned} \quad (46)$$

$$(\bar{\rho} + C_m) \left( \frac{dH_D}{dT} + T \frac{d^2 H_D}{dT^2} \right) = \frac{4\bar{\rho} \bar{Q}_d}{\bar{d}^2} \cos \phi - \frac{\bar{d}}{W_e \bar{Q}_d} \frac{\sin \bar{\Psi}}{\bar{\Psi}} - \frac{T}{F_r} \cos \theta, \quad (47)$$

$$\bar{r}_f = \sqrt[3]{\frac{3}{2} \bar{Q}_d T_f}. \quad (48)$$

The fracture coordinates, the drop radius and the NAPL entrance diameter were all

normalized to the fracture's aperture. Time was scaled by the amount of time it takes the flowing water to traverse a distance equal to the fracture's aperture and the drop's density was normalized against the water's density. The NAPL flow rate was scaled by the water flow rate. The Froude number expresses the magnitude of the water's inertial force relative to the buoyancy force generated by the drop and the Weber number expresses the magnitude of the water's inertial force relative to the drop's surface tension force.

## 5. Final drop size analysis

For this analysis, it is assumed that the drop initially begins its formation process in the expansion stage. The expansion stage begins when the NAPL initially enters into the fracture. This stage is characterized mainly by the drop's base remaining in constant contact with the fracture wall. The base does not lift from the wall due to the normal component of the net force acting on the drop,  $\vec{F}_n$ , is less than zero. Therefore, the drop's center coordinate  $H_D$  is equivalent to the radius of the drop (see Figure 4). This simplifies equation (47) as both the first and second derivatives of  $H_D$  can now be obtained analytically by taking these derivatives of the following expression for  $H_D$

$$H_D = \frac{1}{2} \sqrt[3]{\frac{3}{2} \overline{Q}_d T}, \quad (49)$$

where  $H_D$  was derived from the equation for the volume of a sphere. Utilizing the first and second derivatives of equation (49) and setting the sum of the forces in equation

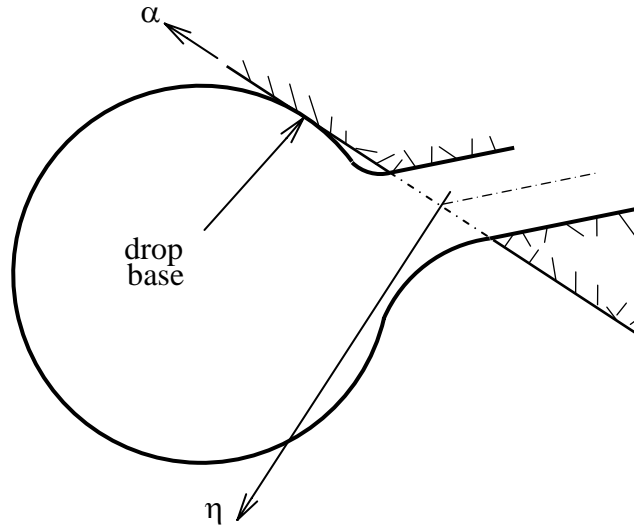


**Figure 4. Schematic representation of a drop during the expansion stage**

(47) to less than or equal to zero gives a relationship which holds true throughout the expansion stage of a forming drop

$$\frac{3}{54} C_m \sqrt[3]{\frac{3\bar{Q}_d}{2}} T^{-\frac{2}{3}} \geq \frac{\bar{\rho}\bar{Q}_d}{\bar{d}^2} \cos \phi - \frac{4\bar{d}}{W_e \bar{Q}_d} \frac{\sin \bar{\Psi}}{\bar{\Psi}} + \frac{1}{F_r} T \cos \theta . \quad (50)$$

This relationship is only valid during the expansion stage. Once equation (50) is violated the drop has begun to lift from the fracture wall and the drop has entered into the detachment stage. During these initial steps of analysis, equation (50) must always be checked to make sure that it is still valid so that equation (49) can still be used for this portion of the computations.

The goal of this analysis is to determine the specific time during the drop formation process when equation (45) becomes valid. To do this the coordinates  $A_D$  and  $H_D$  must be determined at each time step used in the calculation. During the expansion stage equation (49) can be used to determine the value of  $H_D$ .  $A_D$  can be calculated

from equation (46) and this is done by the use of a fourth-order Runge-Kutta numerical method [Kreyszig, 1993].  $H_D$  and  $A_D$  are calculated from these equations at each time step until either equation (45) becomes true or equation (50) becomes invalid. If equation (45) becomes true first then the drop has severed its neck and has completed its growth cycle, thus reaching its final size. If equation (50) becomes invalid before (45) becomes valid then the drop has entered into the detachment stage and  $H_D$  must now be calculated from equation (47) using the same fourth-order Runge-Kutta numerical method used for calculating  $A_D$ . New values are calculated for  $A_D$  and  $H_D$  at each time step until equation (45) is validated and at this point in time the drop has severed its neck and has reached its final size.

## 6. Drop size results and discussion

The drop sizing model presented in this work, equations (45) through (48), is similar to a model derived by Kim et al., 1994 for a bubble forming in a flowing liquid. The significant difference between the models is that equation (46) uses a curve fitted drag coefficient, equation (12), compared to the drag coefficient for a drop free falling through a continuous phase used by Kim. This coefficient is given by

$$C_D = \frac{8}{\text{Re}} \left( \frac{2 + 3\bar{\mu}}{1 + \bar{\mu}} \right) \quad \text{Re} \leq 4, \quad (51)$$

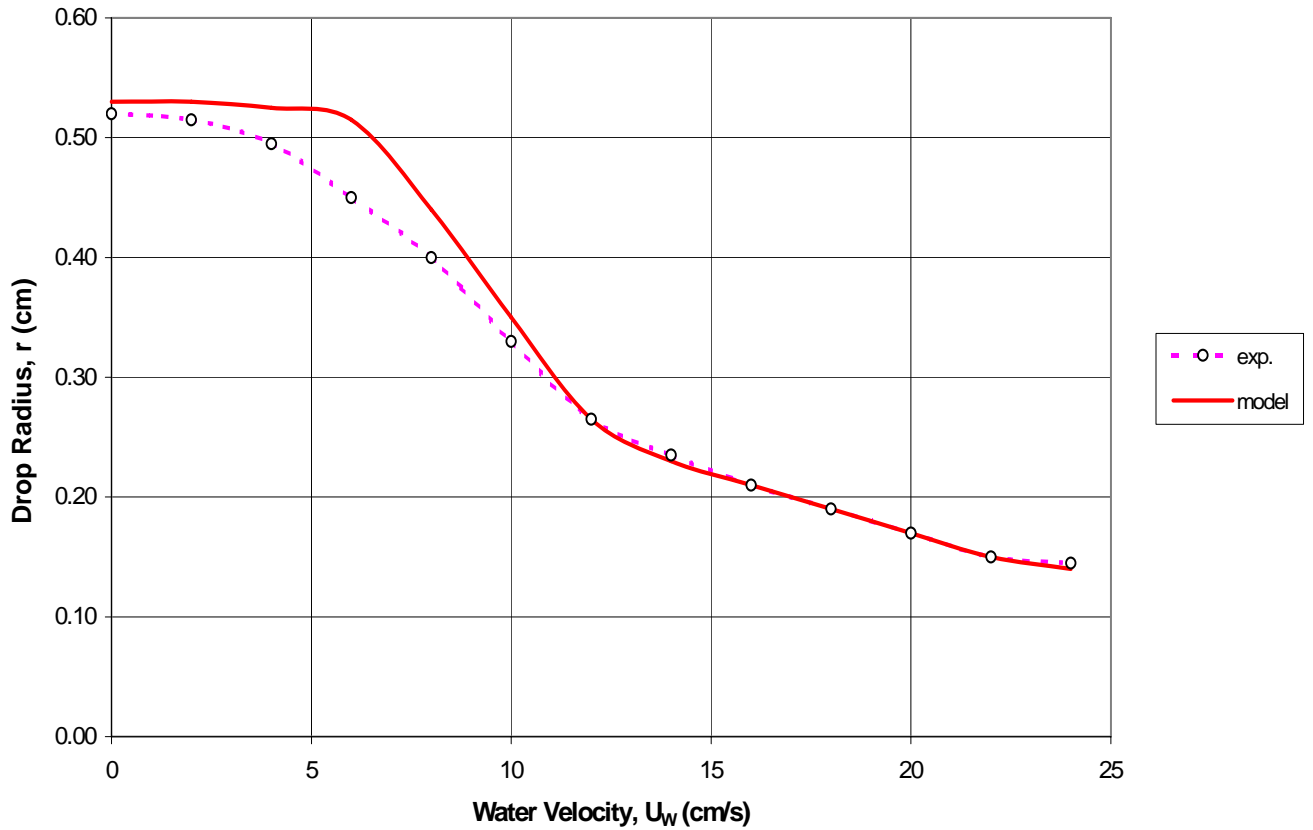
where  $\bar{\mu}$  is the viscosity ratio given by  $\bar{\mu} = \frac{\mu_D}{\mu_w}$ .  $\mu_D$  is the absolute viscosity of the

NAPL. At Reynolds numbers much less than one both of these drag coefficients are approximately the same, however equation (51) tends toward zero significantly quicker as Re increases much above one. Equation (46) was chosen over equation (51) because

it follows very closely the experimental data used in determining the value for this drag coefficient over a much larger range of Reynolds numbers [White, 1991]. This work is also modeling a different physical system than Kim team model. The physical system modeled in this work is of a two phase liquid drop formation into a rather narrow channel of flowing water as compared to the Kim team, which focused on air bubble formation in a rather large container of moving water.

In order to test the capabilities of this model, an analysis was performed comparing the drop sizes predicted from this model and data generated from experiments performed by Itoh et al. [1980]. This experiment consisted of a small nozzle, which was used to inject benzene into a fluid contained within a large open container. The experiment was configured so that water could be put into motion within the container while the small nozzle injected the benzene into the moving water from the bottom of the container. Both the benzene and water flow rates were adjustable while the injection nozzle diameter and the depth and width of the flowing water remained constant through out the extent of each experiment. Measurements were taken comparing the drop sizes created at the different water and benzene flow rates. Comparing the drop sizes calculated from equations (45) through (48) with the experimental data requires that the variables used in the equations are set to match its equivalent experimental parameter. For example the NAPL entrance diameter variable was set to match the nozzle diameter and the fracture aperture dimension was set to the depth of the water within the open container. The appropriate values for the density of benzene and the water-benzene surface tension were also used in the calculations. Figure 5 shows the comparison between the calculated drop diameters and the drop diameters generated by the experiment performed by Itoh et al., 1980.

The comparison shows that in the regions of low or high water flow rates the results from equations (45) through (48) match well with the experimental data. In the region of intermediate water velocities, these equations predict drop sizes, which are somewhat larger than the Benzene drops obtained experimentally. The smaller experimental drop sizes are believed to be due to a non-spherical drop shape at this stage of the experiment [Kim *et al.*, 1994]. Because equations (45) through (48)



provide good agreement with

**Figure 5. Comparison of model predictions and experimental data.**

$$Q_d = 6.95 \times 10^{-3} \text{ cm}^3/\text{s}, \text{ Water-Benzene: } d = 0.102 \text{ cm}$$

these experimental results, these equations are adequate for predicting drop sizes in a flowing liquid system.

Two different scenarios were analyzed with the use of the drop-sizing equations (45) through (48). The first system examined was how the final drop radius ratio,  $\bar{r}$ , changed while varying the aperture ratio,  $\bar{d}$ . This comparison was done using two different NAPLs, trichloroethylene (TCE) and dichloromethane (DCM). The flow rates for both the NAPL intrusion and the water inside the fracture were held constant. The results of this analysis are presented in Figure 6 and show that for each variation of  $\bar{r}$  the drop sizes generated were on the same order as  $\bar{r}$ . The drop radius ratios the

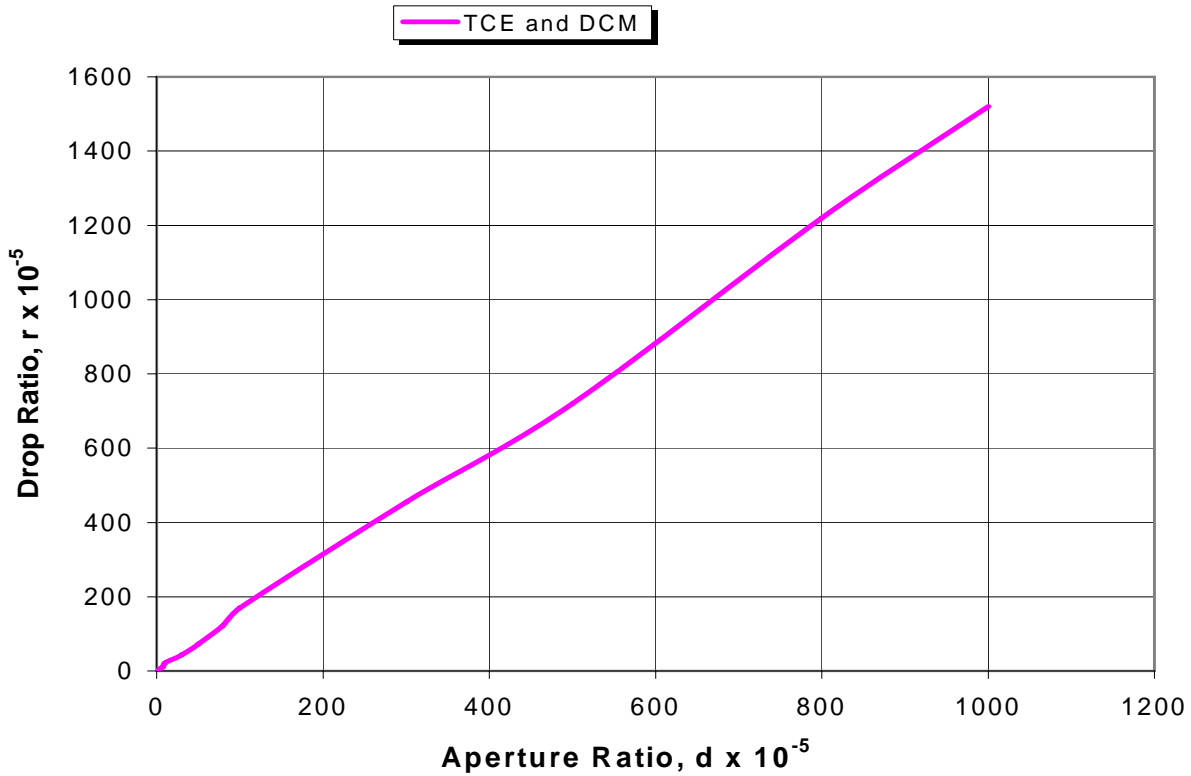


**Figure 6. Comparison of the drop ratio,  $\bar{r}$ , with a changing aperture ratio,  $\bar{d}$ , for TCE and DCM.  $\bar{Q}_d = 1.27 \times 10^{-2}$ ,  $\phi = 90^\circ$ ,  $W_e = 5.68$  and  $\theta = 0^\circ$**

model generated were approximately 1.5 times the NAPL entrance ratios used. This, in essence, means that the size of the drops created within a fractured medium are to be on the order of 1.5 times the size of the NAPL's entrance dimension. Also of interest is that both TCE and DCM generated the same size drops under the given conditions of the analysis. This seems to indicate that drag force probably contributes the most in determining the final size of drop as it appears the different NAPL densities and surface tension values had little effect on final drop radius.

The next system examined was the variance in the drop radius ratio,  $\bar{r}$ , while changing the NAPL flow rate ratio,  $\bar{Q}_d$ . This comparison was done using two different NAPL's, trichloroethylene (TCE) and dichloromethane (DCM) while holding the aperture ratio,  $\bar{d} = .01$ , constant. The results of this analysis are presented in Figure 7 and suggest that the drop ratio  $\bar{r}$  increases with increasing  $\bar{Q}_d$ . What is most interesting is that the drop ratio for both TCE and DCM increases only slightly even though the NAPL flow rate is increased by a magnitude of 4. This seems to indicate that increasing the momentum of the incoming NAPL has a minimal effect on the final size of the drop. Also lower NAPL densities will generate larger drops. This is because the denser drops will detach from the fracture wall sooner due to the larger buoyancy force acting on the drop trying to pull the drop away from the fracture wall.

What is clear when looking at the two scenarios previously outlined is that the two most important forces driving the final sizing of these drops are the drag force and the buoyancy force, as the other forces play a minor, if not insignificant role in creating a drop within a flowing fluid. The size of the drops generated within the fracture are approximately the size of their entrance aperture and therefore will most likely be quite

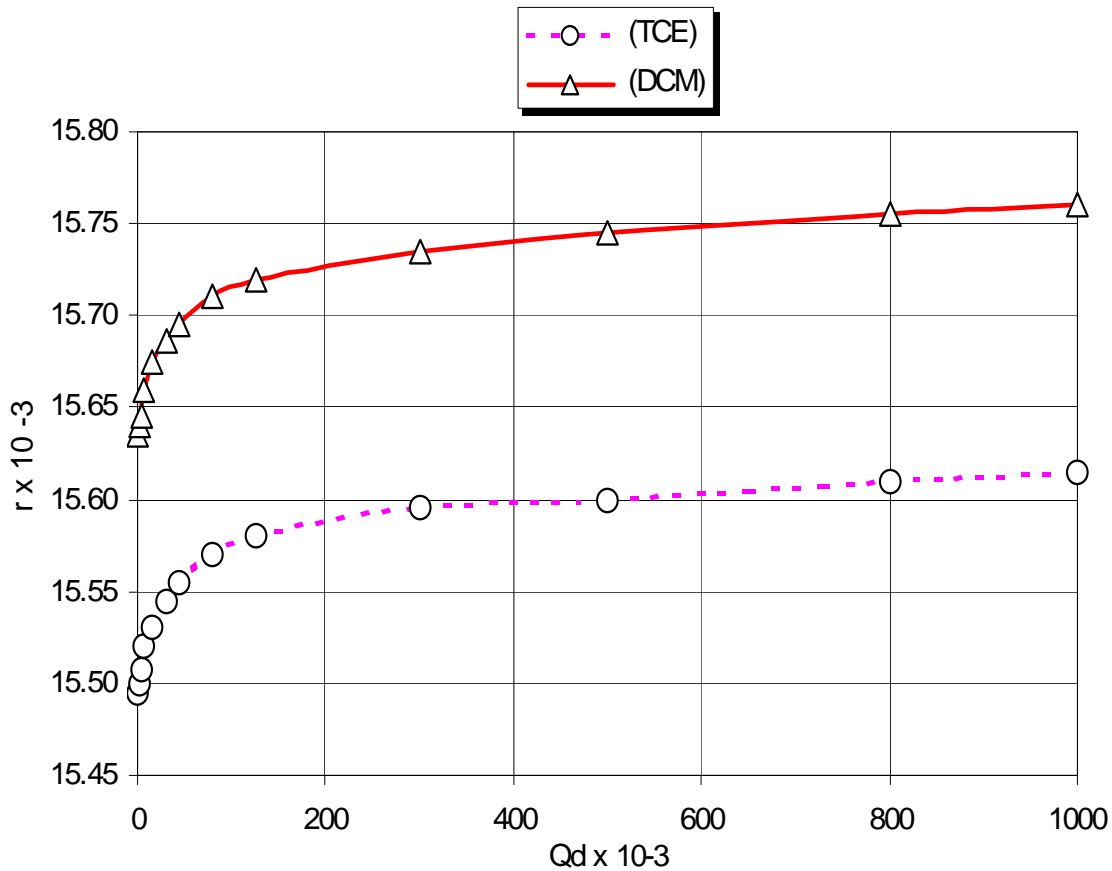


**Figure 7. Comparison of  $\bar{r}$  with a changing NAPL flow rate ratio,  $\bar{Q}_d$ , for TCE and DCM.  $\bar{d} = .01$ ,  $\phi = 90^\circ$ ,  $W_e = 5.68$ ,  $\theta = 0^\circ$**

small since the pore sizes in these locations can be on the order of micrometers. However, there are several pores in which the NAPL may use in order to enter into the fracture, so there is the potential of creating a significant number of small NAPL drops which are able to detach from the fracture walls and enter into the main flow stream. If this is the case then a significant amount of contaminant may find a means in which to further penetrate into the subsurface and become much more difficult to remove.

## 7. Drop motion within a fracture

Once a drop detaches from a fracture wall, it will enter into the interstitial fluid contained within the fracture. If this fluid is moving the drop will migrate along the fracture following a path similar to the one the interstitial fluid takes as it moves through the fracture array. The buoyancy and drag forces have the most effect on the drop and these are the driving forces in dictating the drop's movement within the fracture. The other forces that aided in the formation of the drop, such as the surface tension and momentum forces, no longer have an effect on the drop's motion because the drop is either no longer attached to its initial source of material or the wall of the fracture. Inertial forces still act on the drop however these forces are active only when the drop is accelerating within the interstitial fluid itself, such as when the drop is either detaching from, or attaching to, the fracture walls. However once the drop has entered into the main flow of the fracture it will reach a terminal velocity within the moving water and these inertial forces will no longer exist.

The drop's two-dimensional terminal velocity vector can be calculated by using Newton's 2<sup>nd</sup> Law of motion. When the drop reaches this velocity the drop is no longer experiencing any acceleration and the net force acting on the drop is zero. The only forces acting on the drop at this time are the drag and buoyancy forces and because their net sum is zero they must be balancing each other (see Figure 8). Newton's 2<sup>nd</sup> Law

gives the following relationship

$$\vec{F}_D = -\vec{F}_B. \quad (52)$$

The expressions for these two forces are obtained from equations (9) and (5)

respectively. This leads to the following expressions

$$\vec{F}_B = \frac{4\pi r^3}{3} g(\rho_d - \rho_w)(\hat{\eta} \cos \theta - \hat{\alpha} \sin \theta), \quad (53)$$

$$\vec{F}_D = \frac{\pi}{2} C_{dw} \rho_w r^2 \{U_\alpha^2 \hat{\alpha} - U_\eta^2 \hat{\eta}\}, \quad (54)$$

where  $U_\alpha$  is the effective velocity in the  $\alpha$  direction and  $U_\eta$  is the effective velocity in the  $\eta$  direction. The drop's effective area,  $A_{eff}$ , used in deriving equation (54) is defined by equation (11) and the angular offset angle,  $\theta$ , is to be kept between  $0^\circ$  and  $90^\circ$ . This eliminates the absolute value sign required by equation (15), because  $\vec{U}_{eff}$

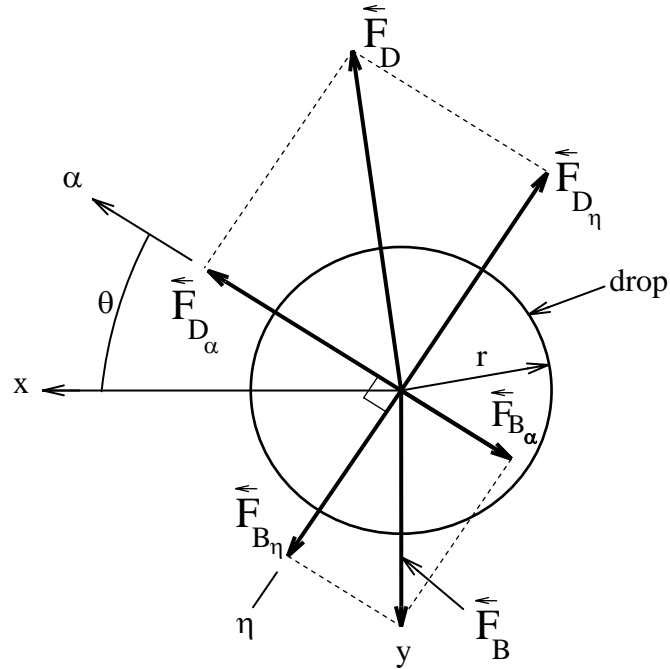


**Figure 8. Macroscopic forces acting on a drop moving within a fracture.**

will always be positive. The drop's volume is assumed to remain constant, though the drop is continuously diffusing as it migrates within the fracture. This assumption is

valid due to the fact the amount of mass transferring from the drop into the interstitial fluid is negligible because of the extremely small value for the mass transfer rate constant that non- aqueous phase liquids possess. Also the drop can not grow larger because it is no longer attached to its NAPL source. The drop's volume is set equal to the volume of a sphere with a radius of  $r$ .

The effective velocity,  $\vec{U}_{eff} = U_\alpha \hat{\alpha} + U_\eta \hat{\eta}$ , is equal to the water velocity in the fracture,  $\vec{U}_w$ , minus the drop velocity,  $\vec{U}_D$ , where

$$\vec{U}_D = U_{D\alpha} \hat{\alpha} + U_{D\eta} \hat{\eta}, \quad (55)$$

$$\vec{U}_w = U_{\max} \left( 1 - \frac{(D-\eta)^2}{D^2} \right) \hat{\alpha} \quad [White, 1991]. \quad (56)$$

$U_\alpha$  is the effective velocity in the  $\alpha$  direction,  $U_\eta$  is the effective velocity in the  $\eta$  direction and  $U_{\max}$  is the maximum water velocity. It is assumed that the water velocity within the fracture is idealized as a Poiseuille Flow, which gives a parabolic velocity profile. Subtracting equation (55) from (56) yields the effective velocity equation

$$\vec{U}_{eff} = U_\alpha \hat{\alpha} + U_\eta \hat{\eta} = \left\{ U_{\max} \left( 1 - \frac{(D-\eta)^2}{D^2} \right) - U_{D\alpha} \right\} \hat{\alpha} - U_{D\eta} \hat{\eta}. \quad (57)$$

Inserting the vector components of equation (57) into (54) and then inserting this equation plus equation (53) into (52) yields

$$\begin{aligned} \frac{\pi}{2} C_{dw} \rho_w r^2 \left( U_{\max} \left( 1 - \frac{(D-\eta)^2}{D^2} \right) - U_{D\alpha} \right)^2 \hat{\alpha} - \frac{\pi}{2} C_{dw} \rho_w r^2 U_{D\eta}^2 \hat{\eta} = \\ = -\frac{4}{3} \pi r^3 (\rho_d - \rho_w) g (\hat{\eta} \cos \theta - \hat{\alpha} \sin \theta). \end{aligned} \quad (58)$$

Breaking equation (58) into its separate coordinates and simplifying give the final drop velocity equations

$$\hat{\alpha} \text{ direction: } U_{D\alpha} = U_{\max} \left( 1 - \frac{(D-\eta)^2}{D^2} \right) - \sqrt{\frac{8r(\bar{\rho}-1)g}{3C_{dw}}} \sin \theta, \quad (59)$$

$$\hat{\eta} \text{ direction: } U_{D\eta} = \sqrt{\frac{8r(\bar{\rho}-1)g}{3C_{dw}}} \cos \theta. \quad (60)$$

## 8. Advection dispersion equation for a migrating NAPL drop

When a NAPL drop enters into the main flow stream, not only does the drop travel within the fracture array, it also creates a contaminant plume that migrates along with it. The plume is created by NAPL dissolving from the drop's surface and into the surrounding interstitial fluid with diffusion and advection driving the growth and movement of the plume. Therefore, an advection dispersion equation can be employed to describe the movement and fate of a contaminant plume as it migrates and grows within the fracture. The advection dispersion equation is a mass balance equation and can be expressed as [Bear and Verruijt, 1987]

$$\frac{\partial C}{\partial t} = -\vec{\nabla} \bullet \left[ C\vec{U}_{eff} - \tilde{\tilde{D}} \bullet \vec{\nabla} C \right] + \xi_p, \quad (61)$$

where  $C$  is the solute concentration within the water phase,  $\tilde{\tilde{D}}$  is the hydrodynamic dispersion coefficient matrix and  $\xi_p$  is the solute source function. This equation equates the change, with respect to time, of the NAPL concentration within the interstitial fluid to the contributions created by diffusion, movement of the fluid and a NAPL source.

In order to create a working model, the system to be analyzed needs to be defined.

The NAPL drops created within a fracture have diameters of approximately 1.5 times NAPL entrance aperture, therefore a small NAPL entrance point will create small drops. The majority of entrance points into a fracture are from the pores contained within the medium where the fracture exists and there are a significant number of pores which can line the fracture wall. These pore sizes are typically on the order of micrometers or smaller. Fractures, on the other hand, can have aperture which measure in the millimeter range with lengths and depths which can be several meters wide. The majority of the drops formed within a fracture will be several orders of magnitude smaller than the fracture's dimensions. Because the size of these NAPL drops can become quite small what is of initial interest is determining the potential size a contaminant plume generated from one of these drops can grow to. Equation (61) is going to be used to develop a model which will determine the contaminant plume generated from a small drop which exists in a fracture which is significantly larger than the drop.

In order to analyze equation (61) all of the system boundaries and assumptions must first be defined. The first assumption to be made is that once the drop has entered into the fracture's flow stream that the drop will tend to stay in the flow path and develop a contaminant plume before it reattaches somewhere else within the fracture. It is also assumed that the fracture is significantly larger than the drop and that drop, with its contaminant plume, does not interact with the fracture walls. This assumption is based on the belief that the plume generated from these small drops is also very small a will be significantly smaller than the fracture's aperture. The depth of the fracture is neglected and this model will only be considered in two spatial dimensions using the fracture coordinate system of  $\alpha$  and  $\eta$ . The interstitial fluid is water and the water's

velocity is assumed to flow only in the  $\alpha$  direction and have a magnitude of  $U_{\max}$ . The diffusion matrix  $\tilde{D}$  is assumed to be constant in all directions and the fracture is orientated in the horizontal.

With the physical system now defined the next step is integrate the assumptions made into equation (61). Expanding equation (61) into the fracture's coordinates and applying these assumptions yields

$$\frac{\partial C}{\partial t} = D \frac{\partial^2 C}{\partial \alpha^2} + D \frac{\partial^2 C}{\partial \eta^2} - \frac{\partial}{\partial \alpha} (U_{\max} C) - \frac{\partial}{\partial \eta} (U_{\eta} C) + \xi_p, \quad (62)$$

where  $\xi_p$  is the NAPL source function and  $D$  is the constant hydrodynamic dispersion coefficient. The function  $\xi_p$ , is required in order to account for the only NAPL source considered within the fracture which is the diffusing drop. This function shall state the source location and the rate at which a NAPL concentration is input into the water moving within the fracture. To determine this function, specific assumptions are required in order as to define  $\xi_p$ . Because the drop size is assumed to be significantly smaller than the domain in which it interacts, the diffusing drop is assumed to be a point source of NAPL solute. The geometry of a small drop can be approximated to be the size of a square of dimensions  $\Delta\alpha \times \Delta\eta$  where  $\Delta\alpha = \Delta\eta \approx 2r$  (see Figure 9). This allows the perimeter of the drop to be approximated by  $8r$  and the drop's area by  $\Delta\alpha \times \Delta\eta$ . These dimensions are used in determining the NAPL source function,  $\xi_p$ .

The NAPL concentration at the edge of the drop is assumed to be the aqueous saturation concentration,  $C_s$ . The rate of NAPL mass diffusing from the drop can now be calculated by first multiplying  $C_s$  by the drop's perimeter,  $8r$ , and by the mass

transfer rate coefficient,  $\kappa$ . Dividing this quantity by the area surrounding the drop,

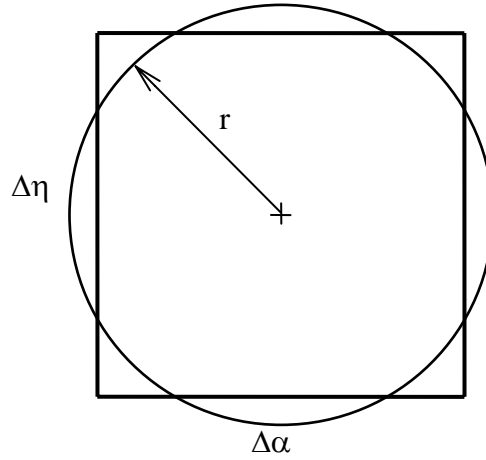


**Figure 9. Drop geometry used for modeling the NAPL source.**

$\Delta\alpha \times \Delta\eta$ , yields the NAPL source concentration flow rate equation

$$\xi_p = \frac{8r\kappa C_s}{\Delta\alpha\Delta\eta} f(\alpha_D, \eta_D), \quad (63)$$

where  $f(\alpha_D, \eta_D)$  is a function which locates the drop in two-dimensional space.

To complete the source function analysis, a function  $f(\alpha_D, \eta_D)$  needs to be determined. This function must locate the drop within the fracture's coordinate system, be dimensionless and have a magnitude of one. A unit step function is used to accomplish this task. The unit step function,  $u(x-x_0)$ , is a dimensionless function which is equal to one for all values of  $x$  greater than or equal to  $x_0$  and zero everywhere else. By combining two of these functions in each dimension and multiplying them together a function  $f(\alpha_D, \eta_D)$  can be created which has a value of one over the spatial area contained by the drop and zero everywhere outside the drop. This function

becomes

$$f(\alpha_D, \eta_D) = \left\{ u \left( \alpha - \left( \alpha_D - \frac{\Delta\alpha}{2} \right) \right) - u \left( \alpha - \left( \alpha_D + \frac{\Delta\alpha}{2} \right) \right) \right\} \times \\ \times \left\{ u \left( \eta - \left( \eta_D - \frac{\Delta\eta}{2} \right) \right) - u \left( \eta - \left( \eta_D + \frac{\Delta\eta}{2} \right) \right) \right\}. \quad (64)$$

Equation (64) can be further simplified by dividing  $f(\alpha_D, \eta_D)$  by the drop area  $\Delta\alpha\Delta\eta$  and using the definition of the Dirac delta function

$$\delta(x - x_0) = \lim_{\Delta x \rightarrow 0} \frac{1}{\Delta x} \left\{ u \left[ x - \left( x_0 - \frac{\Delta x}{2} \right) \right] - u \left[ x - \left( x_0 + \frac{\Delta x}{2} \right) \right] \right\} \quad (65)$$

Applying equation (65) to (64) and inserting into equation (63) yields the final form of the NAPL source function

$$\xi_p = 8r\kappa C_s \delta(\alpha - \alpha_D, \eta - \eta_D). \quad (66)$$

Substituting (66) into equation (62) gives the final form of the Advection-Dispersion equation

$$\frac{\partial C}{\partial t} = D \frac{\partial^2 C}{\partial \alpha^2} + D \frac{\partial^2 C}{\partial \eta^2} - \frac{\partial}{\partial \alpha} (U_{\max} C) - \frac{\partial}{\partial \eta} (U_{\eta} C) + 8r\kappa C_s \delta(\alpha - \alpha_D, \eta - \eta_D). \quad (67)$$

In order to simplify the analysis of equation (67) a change to a different coordinate system is adopted. The new coordinate system's origin is centered on the drop's center and moves with the drop as it migrates within the fracture (see figure 10). The new drop coordinate system variables are defined as

$$\omega = \alpha - U_{D\alpha} t, \quad (68)$$

$$\lambda = \eta - U_{D\eta} t. \quad (69)$$

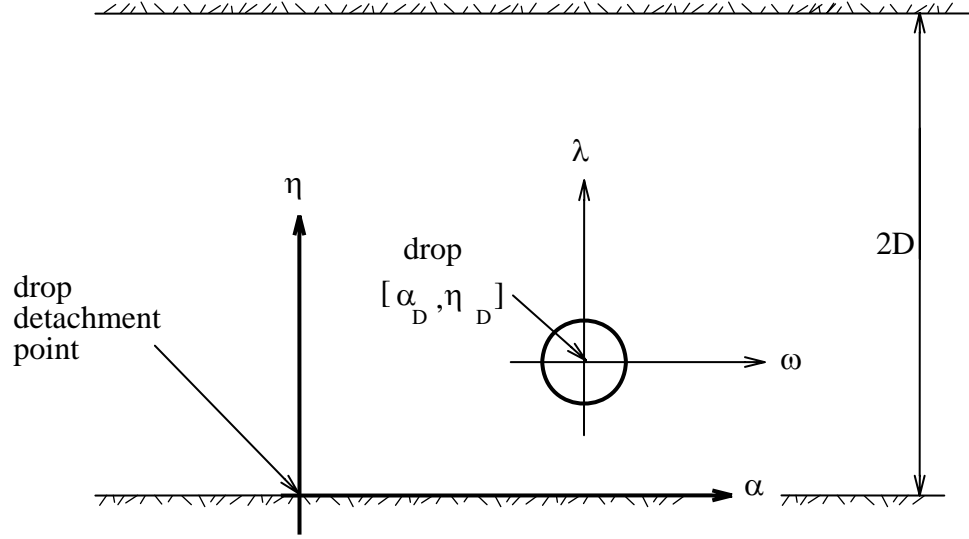


**Figure 10. Coordinate system centered and moving with the drop.**

The effective velocities,  $U_{\max}$  and  $U_{\eta}$ , do not change in the new coordinate system.

Converting equation (67) into the new coordinate system yields

$$\frac{\partial C}{\partial t} = D \frac{\partial^2 C}{\partial \omega^2} + D \frac{\partial^2 C}{\partial \lambda^2} - U_{\max} \frac{\partial C}{\partial \omega} - U_{\eta} \frac{\partial C}{\partial \lambda} + 8r\kappa C_s \delta(\omega, \lambda). \quad (70)$$

Initially, there is no NAPL concentration anywhere within the fracture. This initial condition can be stated as

$$C(0, \omega, \lambda) = 0. \quad (71)$$

Also, it is assumed that there is no NAPL flux at large distances away from the drop.

These boundary conditions are defined by

$$\frac{\partial C(t, \pm\infty, \lambda)}{\partial \omega} = 0, \quad (72)$$

$$\frac{\partial C(t, \omega, \pm\infty)}{\partial \lambda} = 0. \quad (73)$$

The complete Advection-Dispersion model for a migrating diffusing NAPL drop consists of equations (70) through (73) and can now be solved.

### 9. Solution of the advection dispersion equation for a moving drop

The first step in obtaining a transient solute concentration model solution is to perform two transformations on the governing equations (70) through (73). The first transformation performed on these equations is a Fourier Transform with respect to the spatial coordinate,  $\omega$ , by utilizing the following definitions [Farlow, 1993]

$$\tilde{C}(t, \gamma, \lambda) = \frac{1}{\sqrt{2\pi}} \int_{-\infty}^{\infty} C(t, \omega, \lambda) e^{-i\gamma\omega} d\omega, \quad (74)$$

$$\mathfrak{F}\left\{\frac{dC(t, \omega, \lambda)}{d\omega}\right\} = i\gamma\tilde{C}(t, \gamma, \lambda), \quad (75)$$

$$\mathfrak{F}\left\{\frac{d^2C(t, \omega, \lambda)}{d\omega^2}\right\} = -\gamma^2\tilde{C}(t, \gamma, \lambda), \quad (76)$$

$$\mathfrak{F}\{\delta(\omega)\} = \frac{1}{\sqrt{2\pi}}. \quad (77)$$

Applying these definitions to equations (70) through (73) yields

$$\frac{\partial\tilde{C}}{\partial t} = -D\gamma^2\tilde{C} + D\frac{\partial^2\tilde{C}}{\partial\lambda^2} - i\gamma U_{\max}\tilde{C} - U_{\eta}\frac{\partial\tilde{C}}{\partial\lambda} + 4\sqrt{\frac{2}{\pi}}r\kappa C_s\delta(\lambda), \quad (78)$$

$$\tilde{C}(0, \gamma, \lambda) = 0, \quad (79)$$

$$\frac{\partial\tilde{C}(t, \gamma, \pm\infty)}{\partial\lambda} = 0. \quad (80)$$

The next step is again to perform a Fourier Transform with respect to the spatial coordinate,  $\lambda$ , by utilizing the following definitions [Farlow, 1993]

$$\widehat{C}(t, \gamma, \varepsilon) = \frac{1}{\sqrt{2\pi}} \int_{-\infty}^{\infty} \widetilde{C}(t, \omega, \lambda) e^{-i\varepsilon\lambda} d\lambda, \quad (81)$$

$$\mathfrak{F}\left\{\frac{d\widetilde{C}(t, \omega, \lambda)}{d\lambda}\right\} = i\varepsilon\widehat{C}(t, \gamma, \varepsilon), \quad (82)$$

$$\mathfrak{F}\left\{\frac{d^2\widetilde{C}(t, \omega, \lambda)}{d\lambda^2}\right\} = -\varepsilon^2\widehat{C}(t, \gamma, \varepsilon), \quad (83)$$

$$\mathfrak{F}\{\delta(\lambda)\} = \frac{1}{\sqrt{2\pi}}. \quad (84)$$

Applying these definitions to equations (78) through (80) yields

$$\frac{d\widehat{C}}{dt} = -Z_1\widehat{C} + \frac{4}{\pi}r\kappa C_s \quad (85)$$

where

$$Z_1 = \mathcal{D}(\gamma^2 + \varepsilon^2) + i(U_{\max}\gamma + U_{\eta}\varepsilon), \quad (86)$$

$$\widehat{C}(0, \gamma, \varepsilon) = 0. \quad (87)$$

The resulting transformed equation (85) is a non-homogeneous ODE with equation (87) as its initial condition. The general solution for a non-homogeneous ODE of the form

$$\frac{dy}{dt} + p(t)y = r(t) \text{ is [Kreyszig, 1988]}$$

$$y(t) = e^{-h} \left( \int e^h r(t) dt + c \right) \quad (88)$$

where

$$h = \int p(t) dt. \quad (89)$$

Using equations (88) and (89) to solve equation (85) and applying the initial condition equation (87) gives

$$\widehat{C} = \frac{4rkC_s}{\pi Z_1} (1 - e^{-Z_1 t}). \quad (90)$$

Now equation (90) can be rewritten by utilizing the following relationship

$$\frac{1}{Z_1} (1 - e^{-Z_1 t}) = \int_0^t e^{-Z_1 \tau} d\tau. \quad (91)$$

Inserting equation (91) into (90) will help in performing the inverse transformations needed to get to the final solution. Inserting this equation and (86) into (90) yields

$$\widehat{C} = \frac{4rkC_s}{\pi} \int_0^t \exp\left\{-\left(\mathcal{D}\varepsilon^2 + iU_\eta \varepsilon\right)\tau - \left(\mathcal{D}\gamma^2 + iU_{\max} \gamma\right)\tau\right\} d\tau. \quad (92)$$

The next step in finding the solution to the model is to perform two inverse Fourier Transforms on equation (92). For the first inverse transformation the following definitions are used [Farlow, 1993]

$$\mathfrak{F}^{-1}\left\{\frac{1}{a\sqrt{2}} e^{-\frac{\varepsilon^2}{4a^2}}\right\} = e^{-a^2 \lambda^2}, \quad (93)$$

$$\mathfrak{F}^{-1}\left\{\frac{1}{\sqrt{2\pi}} e^{-ia\varepsilon}\right\} = \delta(\lambda - a), \quad (94)$$

$$\mathfrak{F}^{-1}\{\mathfrak{F}(f)\mathfrak{F}(g)\} = f(\lambda) \circ g(\lambda) = \frac{1}{\sqrt{2\pi}} \int_{-\infty}^{\infty} f(\lambda - \chi)g(\chi) d\chi \quad (95)$$

Applying equations (93) and (94) to the appropriate portions of equation (92) gives the following

$$\mathfrak{F}^{-1}\left\{e^{-\mathcal{D}\tau\varepsilon^2}\right\} = \sqrt{\frac{1}{2\mathcal{D}\tau}} e^{-\frac{\lambda^2}{4\mathcal{D}\tau}}, \quad (96)$$

$$\mathfrak{F}^{-1}\left\{e^{-iU_\eta \tau\varepsilon}\right\} = \sqrt{2\pi} \delta(\lambda - U_\eta \tau). \quad (97)$$

To complete the first initial transformation the convolution of equations (96) and (97)

must be calculated.

$$\begin{aligned} f(\lambda) \circ g(\lambda) &= \sqrt{\frac{1}{2D\tau}} \int_{-\infty}^{\infty} \delta(\chi - U_{\eta}\tau) \exp\left\{-\frac{(\lambda - \chi)^2}{4D\tau}\right\} d\chi \\ &= \sqrt{\frac{1}{2D\tau}} \exp\left\{-\frac{(\lambda - U_{\eta}\tau)^2}{4D\tau}\right\}. \end{aligned} \quad (98)$$

Using the results from equation (98) and applying them to (92) yields

$$\tilde{C}(t, \gamma, \lambda) = \frac{4rkC_s}{\pi\sqrt{2D}} \int_0^t \frac{1}{\sqrt{\tau}} \exp\left\{-\frac{(\lambda - U_{\eta}\tau)^2}{4D\tau}\right\} \exp\{- (D\gamma^2 + iU_{\max}\gamma)\tau\} d\tau. \quad (99)$$

The final step in determining the solution to the model is perform another inverse Fourier Transforms on equation (99). For the final inverse transformation the following definitions are used [Gradshteyn, 1980]

$$\mathfrak{F}^{-1}\left\{\frac{1}{a\sqrt{2}} e^{-\frac{\gamma^2}{4b^2}}\right\} = e^{-b^2\omega^2}, \quad (100)$$

$$\mathfrak{F}^{-1}\left\{\frac{1}{\sqrt{2\pi}} e^{-ib\gamma}\right\} = \delta(\omega - b), \quad (101)$$

$$\mathfrak{F}^{-1}\{\mathfrak{F}(f)\mathfrak{F}(g)\} = f(\omega) \circ g(\omega) = \frac{1}{\sqrt{2\pi}} \int_{-\infty}^{\infty} f(\omega - \chi)g(\chi)d\chi. \quad (102)$$

Applying equations (100) and (101) to the appropriate portions of equation (99) gives the following

$$\mathfrak{F}^{-1}\left\{e^{-D\tau\gamma^2}\right\} = \sqrt{\frac{1}{2D\tau}} e^{-\frac{\omega^2}{4D\tau}}, \quad (103)$$

$$\mathfrak{F}^{-1}\left\{e^{-iU_{\max}\tau\gamma}\right\} = \sqrt{2\pi}\delta(\omega - U_{\max}\tau). \quad (104)$$

To complete the final transformation the convolution of equations (103) and (104) must be calculated.

$$\begin{aligned}
f(\omega) \circ g(\omega) &= \sqrt{\frac{1}{2D\tau}} \int_{-\infty}^{\infty} \delta(\chi - U_{\max}\tau) \exp\left\{-\frac{(\omega - \chi)^2}{4D\tau}\right\} d\chi \\
&= \sqrt{\frac{1}{2D\tau}} \exp\left\{-\frac{(\omega - U_{\max}\tau)^2}{4D\tau}\right\}.
\end{aligned} \tag{105}$$

Using the results from equation (105) and applying them to (99) yields

$$C(t, \omega, \lambda) = \frac{2rkC_s}{\pi D} \int_0^t \frac{1}{\tau} \exp\left\{-\frac{(\lambda - U_{\eta}\tau)^2}{4D\tau}\right\} \exp\left\{-\frac{(\omega - U_{\max}\tau)^2}{4D\tau}\right\} d\tau. \tag{106}$$

Expanding the square terms in the exponents and simplifying yields the final solution in the drop's coordinate system

$$C(t, \omega, \lambda) = \frac{2rkC_s}{\pi D} \exp\left\{\frac{U_{\eta}\lambda + U_{\max}\omega}{2D}\right\} \int_0^t \frac{1}{\tau} \exp\left\{-\frac{a}{\tau} - b\tau\right\} d\tau, \tag{107}$$

where

$$a = \frac{\lambda^2 + \omega^2}{4D}, \tag{108}$$

$$b = \frac{U_{\max}^2 + U_{\eta}^2}{4D}. \tag{109}$$

Equations (107) and (108) can be converted from the drop coordinates,  $\omega$  and  $\lambda$ , into the fracture coordinates,  $\alpha$  and  $\eta$  by replacing the  $\omega$  and  $\lambda$  by equations (68) and (69), respectively.

## 10. Drop and contaminant plume motion results and discussion

A moving NAPL drop and its associated contaminant plume provide an additional means for spreading a contaminant within a porous medium that contains fractures. When a drop enters into a horizontal fracture it will obtain a longitudinal velocity,

$U_{D\alpha}$ , equal to the water's velocity,  $U_{\max}\left(1 - \frac{(D-\eta)^2}{D^2}\right)$ , and a buoyancy driven velocity,  $U_{D\eta}$ , which is directed normal to the fracture's walls and is given by equation (60), with  $\theta$  set equal to zero. As the fracture changes its orientation the longitudinal and normal velocities also change in magnitude as part of the buoyancy driven motion is transferred from the normal direction into the longitudinal direction. When a fracture is orientated purely in the vertical direction the drop will only translate in the longitudinal direction, driven by both the flowing water and the buoyancy force, which now directed entirely along the fracture's longitudinal axis.

The drop's normal velocity for a horizontal fracture can be determined by starting from equation (60) and setting  $\theta = 0$ . An expression for  $C_{dw}$  is required in order to determine the normal velocity  $U_{D\eta}$  and this expression is obtained from equation (14). Because we are assuming that the drop radius is much smaller than the fracture's aperture the quantity  $\bar{r}^2$  is much smaller than 1 and therefore  $C_{dw}$  can be approximated by

$$C_{dw} \approx C_D. \quad (110)$$

$C_{dw}$  can be further simplified by assuming that the Reynolds number for the drop's motion is also much less than 1. Applying this assumption to equation (12), simplifying and inserting into equation (110) yields

$$C_{Dw} \approx \frac{24}{\text{Re}} \text{ for } \text{Re} \ll 1. \quad (111)$$

Because there is no water velocity normal to the fracture wall the effective velocity required in the Reynolds number equation (13) is equal to the drop's normal velocity  $U_{D\eta}$ . Utilizing this relationship, equation (13) now becomes

$$\text{Re} = \frac{\rho_w U_{D\eta} 2r}{\mu_w}. \quad (112)$$

Inserting equation (112) into (111) gives

$$C_{Dw} \approx \frac{12\mu_w}{\rho_w U_{D\eta} r}. \quad (113)$$

Substituting equation (113) into equation (60) yields

$$U_{D\eta} = \sqrt{\frac{2\rho_w U_{D\eta}}{9\mu_w} r^2 (\bar{\rho} - 1)g}. \quad (114)$$

Squaring both sides of equation (114) and solving for  $U_{D\eta}$  gives the final result

$$U_{D\eta} = \frac{2\rho_w}{9\mu_w} r^2 (\bar{\rho} - 1)g. \quad (115)$$

The result obtained in equation (115) show that the drop's normal velocity within a two-dimensional horizontal fracture is proportional to the cross sectional area of the drop. As the size of a drop increases, its normal velocity will also increase by an equal amount. The driving mechanism behind this is the buoyancy force. The buoyancy force, as defined by equation (53), is proportional to drop's volume. Because of this, a larger drop will generate a larger buoyancy force acting on the drop and this induces a larger velocity directed inline with the buoyancy force. In a horizontal fracture this force is directed perpendicular to the fracture walls and therefore only affects the drop's normal velocity. As the fracture deviates from the horizontal the drop's normal

velocity will begin to decrease as the buoyancy force now gains a longitudinal component and begins to affect the drop's longitudinal velocity.

The longitudinal velocity of a drop is given by equation (59) and is equal to the water velocity within the fracture when the fracture's orientation is horizontal. This velocity also is dependent on the orientation of the fracture and can either increase or decrease depending on the angle of inclination of the fracture and the direction of flow. It is possible for a NAPL drop to move in the opposite direction of the fracture's water flow if the component of the buoyancy force, which points in the opposite direction of the flowing water, is strong enough to overcome the moving water. This may happen when water is flowing upward in a severely inclined fracture at a low velocity and a strong buoyancy force, such as the force generated by a large drop, is directed downward. However, a small NAPL drop normally will move along the direction of water flow and follow along as the water moves within the fracture.

Not only will a NAPL drop move as a separate phase inside a fracture but it will also diffuse into the water itself and create a contaminant plume that further enhances the spreading of the NAPL. The rate at which NAPL diffuses from the drop is governed by these four items: the mass transfer coefficient,  $\kappa$ , the drop's radius,  $r$ , the hydrodynamic dispersion coefficient,  $D$  and the aqueous saturation concentration,  $C_s$ . The drop's radius determines the amount of water/drop surface interface area there is available to contribute to the diffusion process and aqueous saturation concentration determines the amount of NAPL solute that is available to be dispersed. Also the mass transfer coefficient value dictates the given rate at which the NAPL mass leaves the drop's surface. How quickly the NAPL spreads into the surrounding water is driven by

the hydrodynamic dispersion coefficient. The larger the value for  $D$ , the quicker the NAPL solute migrates throughout the water's domain. These four parameters coupled together within equation (107) determine the amount and the rate at which NAPL leaves the drop and migrates into its surrounding area.

The extent that the NAPL migrates away from the drop and into the aqueous phase is governed by equation (107) as the solute concentration gradient can be determined from this equation for any given time. Figure 11 shows the expansion of a contaminant plume generated from a single TCE drop calculated at four separate time frames. Each contour line shown in Figure 11 represents the extent the plume has migrated away

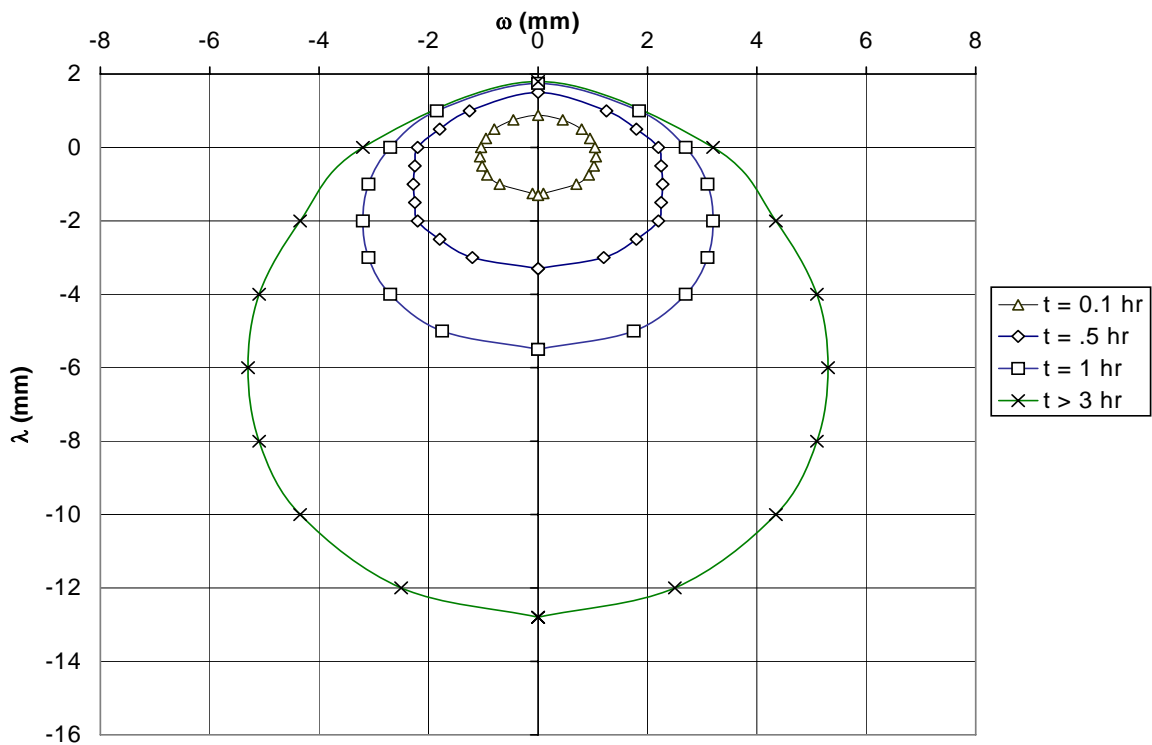


**Figure 11. TCE plumes generated from a single drop within a horizontal fracture at four specific times.**

$$r = 1\mu\text{m}, U_{\alpha} = 0, U_{\eta} = -3.63 \text{ mm/h}, C = 5 \mu\text{g/L}, k = 0.1 \text{ mm/h},$$

$$C_s = 1.1 \text{ g/L}, D = 3.60\text{mm}^2/\text{h}, \rho_{TCE} = 1.46 \text{ kg/L}$$

from the drop, which is located at coordinates [0,0]. The solute concentration measured at these contours is 5 µg/L, which is the maximum limit of TCE allowed in drinking water. The drop has a radius of 1 µm and is moving within a horizontal fracture. The effective normal velocity of the drop is -3.63mm/hr while the effective longitudinal velocity is 0 since the drop will move at the same velocity as the flowing water in the longitudinal direction in a horizontal fracture. This figure shows that the plume remains symmetrical along the normal axis of the fracture, expanding outward from the drop as time increases. As time approaches approximately 3 hours the drop's plume size has stabilized with the furthest distance traveled by the 5 µg/L plume of nearly 13 mm away from the drop. The extent of a stabilized plume can be determined from equation (107) by increasing the time limit in the integral to infinity. This integral is defined as [Gradshteyn and Ryzhik, 1980]

$$\int_0^{\infty} \frac{1}{\tau} \exp\left\{-\frac{a}{\tau} - b\tau\right\} d\tau = 2K_0(2\sqrt{ab}), \quad (116)$$

where  $K_0$  is the modified Bessel function of the second kind and zero order. Substituting (116) into equation (107) yields the final expression for stabilized plume

$$C(t, \omega, \lambda) = \frac{4rkC_s}{\pi D} \exp\left\{\frac{U_\eta \lambda + U_\alpha \omega}{2D}\right\} K_0(2\sqrt{ab}). \quad (117)$$

This result is similar to the results obtained by Bear [1972] for a stationary point source with continuous injection into a two-dimensional porous medium that has stabilized.

The plume generated from a single NAPL drop can grow significantly when it is experiencing effective velocities in both the  $\lambda$  and the  $\omega$  directions. Figure 12 shows

the extent of the plumes generated from a NAPL drop moving within a fracture and is experiencing effective velocities in both directions. Again, the solute concentration measured at these contours is  $5 \mu\text{g/L}$ , the drop radius is held at  $1 \mu\text{m}$  and the effective normal velocity of the drop is  $-3.63\text{mm/hr}$ . Each contour represents the extent of the plume after the plumes have stabilized and are no longer growing. If a drop experiences an additional longitudinal velocity, such as when the drop is traveling within a fracture which is not in the horizontal position, the extent of the NAPL plume

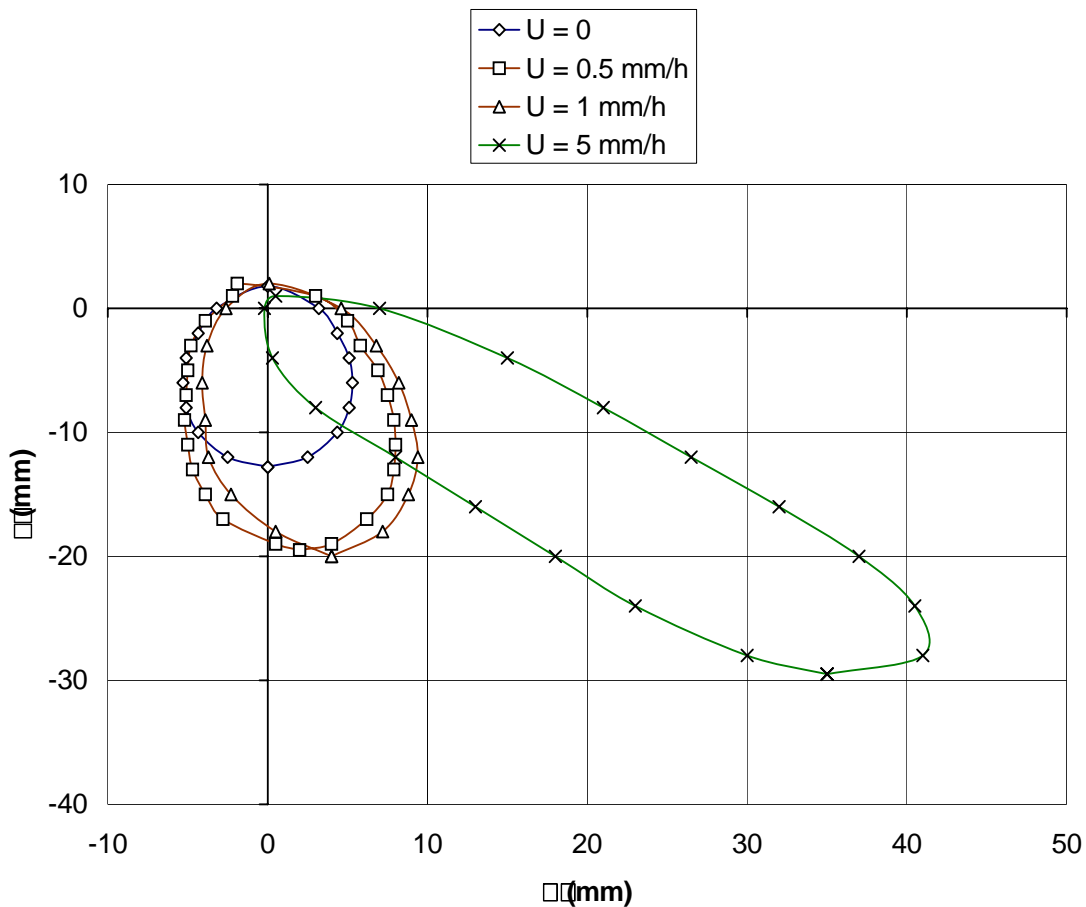


**Figure 12. TCE plumes generated from a single drop within a fracture at four specific longitudinal velocities,  $U_x$ .**

$$r = 1\mu\text{m}, U_y = -3.63 \text{ mm/h}, C = 5 \mu\text{g/L}, k = 0.1 \text{ mm/h}, C_s = 1.1 \text{ g/L},$$

$$D = 3.60\text{mm}^2/\text{h}, \rho_{TCE} = 1.46 \text{ kg/L}$$

grows considerable, as compared to the plume generated from a drop that is experiencing an effective velocity in the normal direction only. The plume generated from the system with the largest longitudinal velocity of 5 mm/h created a plume that experiencing an effective velocity in the normal direction only. The plume generated from the system with the largest longitudinal velocity of 5 mm/h created a plume that spread more than 40 mm in  $\omega$  direction and nearly 30 mm in the  $\lambda$  direction. These distances are significantly larger than the plume generate from the drop experiencing no longitudinal velocity. This larger plume size is driven by the increase in the total effective velocity the drop is experiencing by helping the NAPL solute to move away from the drop quicker. This increases the solute concentration gradient the NAPL drop experiences which enables the drop to diffuse more contaminant at a quicker rate.

## **SUMMARY AND CONCLUSIONS**

The analysis provided in this research focused on the growth, the movement and the diffusion of one NAPL drop contained within the confines of one fracture. The drop sizes generated by equations (45) through (51) were on the order of 1.5 times the NAPL entrance and the two most influential forces driving the final sizing of the drop are the drag force and the buoyancy force acting on the drop during its formation. The surface tension force, the momentum flux force and the induced inertial force have little or no effect on the outcome of the final drop size. NAPLs can enter into a fracture either from another connecting fracture or through the pores contained within the porous medium that connect to the fracture walls. The drops generated from the connecting pores will be very small with diameters that are on the order of microns. Though these drops are extremely small the potential exists that a significant number of these drops can be created due to the fact that there are several pore channels lining the walls of the

fracture. Once the NAPL enters into the fracture it can form several drops which separate from the fracture walls and enter into the fracture's flow stream. These drops can now move deeper into the fractured medium driven by the buoyancy of the drop and the flowing water contained within the fracture array. This mechanism provides another means for a NAPL to migrate within a geologic medium and helps to increase the spreading of the contaminant.

When a NAPL drop enters into the fracture's flow stream it will move within the fracture at velocities given by equations (59) and (60). The drop's velocity is dependant on the NAPLs density, drop size and the velocity of the flowing water. During the drops migration the drop will also diffuse into the water and create a contaminant plume. This plume travels along with the drop and spreads within the fracture. The size and concentration of the contaminant plume is dictated primarily by the size of the drop and the effective velocities the drop sees as it moves through out the fracture.

A two-dimensional advection dispersion equation, equation (70), was derived for a NAPL point source which assumed that the drop and its contaminant plume were so small that they did not interact with the fracture boundaries. This equation, and its associated boundary and initial conditions, was solved using a Fourier Transform and an analytical solution was obtained (equation 107). From this equation two systems were examined with the first being an analysis of the transient plumes generated from a TCE drop with a radius of  $1\mu\text{m}$  moving within a significantly larger horizontal fracture. The second analysis examined the effect different longitudinal velocities had on the growth of the contaminant plume generated from the same drop. Both systems generated stable plumes with concentration contours, representing a 5ppm solute

concentration, traveling from 90mm to over 600mm from the drop. These plume dimensions are significantly larger than the size of a typical fracture where an aperture of 1mm is considered large. Because these plumes are significantly larger than what was anticipated, the initial assumption, which neglected the lack of interaction between the NAPL plume and the fracture walls, was in error. Further study of this system must consider the affect the fracture walls will have on the plume as it is generated from the drop and grows within the fracture. This is accomplished by assuming the boundary condition, equation (73), at the fracture walls is one in which there is no contaminant flux across these boundaries. An analytical solution to equation (70) can then be obtained by first taking a Fourier Transform in the longitudinal direction and then a Finite Cosine Fourier Transform in the normal direction.

## NOTATIONS

$A_D$ direction	dimensionless variable, drop's center in the longitudinal direction
$A_{eff}$	effective area of the drop, $[L^2]$
$A_f$	area of NAPL entrance point, $[L^2]$
$C$	solute concentration within the water phase, $[M/L^3]$
$\tilde{C}$	Fourier transformed solute concentration w. r. t. $\gamma$
$\hat{C}$	Fourier transformed solute concentration w. r. t. $\varepsilon$
$C_D$	curve fit unbounded flow drag coefficient
$C_{dw}$	drag coefficient for a bounded flow
$C_m$	reduced mass coefficient
$C_s$	aqueous saturation concentration (solubility), $[M/L^3]$
$D$	one half the fracture aperture, $[L]$
$\tilde{\tilde{D}}$	hydrodynamic dispersion coefficient matrix, $[L^2/t]$
$\mathcal{D}$	constant hydrodynamic dispersion coefficient, $[L^2/t]$
$d$	diameter of the NAPL entrance point, $[L]$
$\bar{d}$	dimensionless NAPL entrance point diameter
$\mathfrak{F}$	Fourier operator
$\mathfrak{F}^{-1}$	Fourier inverse operator
$F_r$	Froude number
$g$	gravitational acceleration constant, $[L/t^2]$
$H_D$	dimensionless variable, drop's center in the vertical direction
$K_0$	modified Bessel function of the second kind and zero order
$M_r$	reduced mass constant, $[M]$
$Q_d$	constant NAPL volumetric flow rate, $[L^3/t]$
$\bar{Q}_d$	dimensionless NAPL volumetric flow rate
$r$	drop radius, $[L]$
$\bar{r}$	dimensionless drop radius
Re	Reynolds number
$r_f$	final drop radius, $[L]$

$T$	dimensionless time
$\bar{s}$	drop's center position vector, $[L]$
$t$	time, $[t]$
$t_f$	time when drop severs its neck, $[t]$
$\bar{U}_D$	drop velocity vector, $[L/t]$
$U_{D\alpha}$	drop velocity in the longitudinal direction, $[L/t]$
$U_{D\eta}$	drop velocity in the vertical direction, $[L/t]$
$\bar{U}_{eff}$	effective velocity vector, $[L/t]$
$U_{eff}$	magnitude of the effective velocity, $[L/t]$
$U_{max}$	maximum water velocity at the center of the fracture, $[L/t]$
$\bar{U}_w$	water velocity vector within the fracture, $[L/t]$
$U_w$	average water velocity in the fracture, $[L/t]$
$U_\alpha$	effective velocity in the $\alpha$ direction, $[L/t]$
$U_\eta$	effective velocity in the $\eta$ direction, $[L/t]$
$\forall_d$	drop volume, $[L^3]$
$W_e$	Weber number
$x$	spatial coordinate in the longitudinal direction, $[L]$
$\hat{x}$	unit vector the $x$ direction, $[L]$
$y$	spatial coordinate in the vertical direction, $[L]$
$\hat{y}$	unit vector in the $y$ direction, $[L]$

### Greek Letters

$\alpha$	spatial coordinate in the longitudinal direction, $[L]$
$\hat{\alpha}$	unit vector in the $\alpha$ direction, $[L]$
$\alpha_D$	drop's center longitudinal coordinate, $[L]$
$\gamma$	Fourier transform variable
$\delta(x-x_0, y-y_0)$	Two dimensional Dirac delta function, $[L^{-2}]$
$\Delta$	Effective fracture aperture, $[L]$
$\varepsilon$	Fourier transform variable
$\xi_p$	solute source function, $[M/L^3 \cdot t]$
$\eta$	spatial coordinate in the vertical direction, $[L]$

$\hat{\eta}$	unit vector in the $\eta$ direction, $[L]$
$\eta_D$	drop's center vertical coordinate, $[L]$
$\theta$	fracture angular offset
$\kappa$	mass transfer coefficient, $[L/t]$
$\lambda$	drop spatial coordinate in the vertical direction, $[L]$
$\mu$	surface tension coefficient, $[M/t^2]$
$\bar{\mu}$	viscosity ratio
$\mu_D$	absolute viscosity of NAPL $[M/Lt]$
$\mu_w$	absolute viscosity of water $[M/Lt]$
$\bar{\rho}$	dimensionless density
$\rho_d$	NAPL drop density, $[M/L^3]$
$\rho_w$	water density, $[M/L^3]$
$\tau$	dummy integration variable, $[t]$
$\phi$	NAPL entrance angle
$\Psi$	angle of inclination between the drop's center and the $\eta$ axis
$\bar{\Psi}$	dimensionless angle
$\omega$	drop spatial coordinate in the longitudinal direction, $[L]$

## REFERENCES

- Abdel-Salam, A. and Chrysikopoulos, C. V., 1996, Unsaturated flow in a quasi-three-dimensional fractured medium with spatially variable aperture, *Water Resources Research*, **32** (6), 1531-154.
- Abdel-Salam, A. and Chrysikopoulos, C. V., 1994, Analytical solutions for one-dimensional colloid transport in saturated fractures, *Advances in Water Resources*, **17**, 283-296.
- Bear, J., 1972, *Dynamics of Fluids in Porous Media*, American Elsevier Publishing Company, New York.
- Bear, J. and Verruit, A., 1987, *Modeling Groundwater Flow and Pollution*, D. Reidel Publishing Company, Dordrecht, Holland.
- Bellma, L. L. and Kueper, B. H., 1999, Non-wetting phase retention and mobilization in rock fractures, *Water Resources Research*, **35** (7), 2085-2093.
- Beyer, W. H., 1987, *Standard Mathematical Tables, 28<sup>th</sup> Edition*, CRC Press, Inc., Boca Raton, Florida.
- Borhan, A. and Pallint, J., 1998, Pressure driven motion of drops and bubbles through cylindrical capillaries, *Industrial Engineering Chemical Research*, **37**, 3748-3759.
- Chrysikopoulos, C. V. and Abdel-Salam, A., 1997, Modeling colloid transport and dispersion in saturated fractures, *Colloids and Surfaces A: Physicochemical and Eng. Aspects*, **121**, 189-202.
- Chrysikopoulos, C. V., Voudrias, E. A., Fyrrillas, M. M., 1994, Modeling of contaminant transport resulting from dissolution of nonaqueous phase liquid pools in saturated porous media, *Transport in Porous Media*, **16**, 125-145.
- Domenico, P. A. and Schwartz, F. W., 1990, *Physical and Chemical Hydrogeology*, John Wiley & Sons, Inc.
- Farlow, S. J., 1993, *Partial Differential Equations for Scientists and Engineers*, Dover Publications, Inc., New York.
- Feenstra, S. and Cherry, J. A., 1988, Subsurface Contamination by dense non-aqueous phase liquid (DNAPL) chemical. Presented at the International Groundwater Symposium, International Assoc. of Hydrogeologists, Halifax, Nova Scotia, May 1-4.
- Fetter, C. W., 1993, *Contaminant Hydrogeology*, Macmillan, New York.
- Gradshteyn, I. S. and Ryzhik, I. M., 1980, *Tables of Integrals, Series, and Products, Corrected and Enlarged Edition*, Academic Press, Inc., Orlando, Florida

- Itoh, R., Hirata, Y., Inoue, K. and Kitagawa, Y., 1980, Formation of a liquid drop at a single nozzle in a uniform stream, *Int. Chem. Eng.*, **20**, 616.
- James, S. C. and Chrysikopoulos, C. V., 1999, Transport of polydisperse colloid suspensions in a single fracture, *Water Resources Research*, **35** (3), 707-718.
- James, S. C. and Chrysikopoulos, C. V., 2000, Transport of polydisperse colloids In a saturated fracture with spatially variable aperture, *Water Resources Research*, **36** (6), 1457-1465.
- Kawase, Y. and Ulbrecht, J. J., 1981, Formation of drops and bubbles in flowing liquids, *Industrial Eng. Chemical Process Design and Development*, **20**, 636-640.
- Kim, I., Kamotani, Y. and Ostrach, S., 1994, Modeling bubble and drop formation in flowing liquids in microgravity, *AIChE Journal*, **40** (1), 19-28.
- Kim, I., 1992, Modeling of bubble and drop formation in flowing liquids in terrestrial and microgravity environments, *PhD Thesis*, Case Western Reserve Univ., Cleveland, Ohio.
- Kreyszig, E., 1993, *Advanced Engineering Mathematics, 7<sup>th</sup> Edition*, John Wiley & Sons, Inc., New York
- Kuloor, N.R. and Kumar, R., 1990, The formation of bubbles and drops, *Advanced Chemical Engineering*, Academic Press, New York.
- Parker, B. L., Gillham, R. W. and Cherry, J. A., 1994, Diffusive disappearance of immiscible-phase organic liquids in fractured geologic media, *Ground Water*, **32**, 805-820.
- Rubin, H., Rathfelder, K. and Abrida, L. M., 1997, Modeling quasi-steady NAPL dissolution in fractured permeable media, *Journal of Environmental Engineering*, **123** (3), 25-216.
- Tolstov, G. P., 1962, *Fourier Series*, Dover Publications, Inc., New York.
- VanderKwaak, J. E. and Sudicky, E. A., 1996, Dissolution of non-aqueous-phase liquids and aqueous-phase contaminant transport in discretely-fractured porous media, *Journal of Contaminant Hydrology*, **23**, 45-68.
- White, F. M., 1991, *Viscous Fluid Flow, 2<sup>nd</sup> Edition*, McGraw-Hill, Inc., Boston, Massachusetts.